Muscleblind-1, a regulator of alternative mRNA splicing, is required for sensory neuron morphogenesis in *Caenorhabditis elegans*

A Senior Thesis Presented to
The Faculty of the Department of Molecular Biology,
The Colorado College

By

Aidan W. Wells
Bachelor of Arts
Colorado College
May 2024

Darrell J. Killian, Ph.D.
Associate Professor of Molecular Biology, Department Chair
Supervisor, Primary Thesis Advisor

Spencer Gang, Ph.D.
Assistant Professor of Molecular Biology
Secondary Thesis Advisor

ABSTRACT

Neural cells are characterized by their diverse, often highly elaborate, cellular morphologies. The structural diversity within the nervous system provides the functional versatility necessary for the emergence of complex behaviors. Defects in neuronal morphology are associated with neurological disorders; therefore, understanding the molecular mechanisms that establish neuronal architecture has important implications for human health and disease. The *Caenorhabditis elegans* multidendritic sensory PVD neurons, which structurally resemble mammalian polymodal nociceptors, are a popular model for studying neuronal morphogenesis *in vivo*. Based on recent studies, post-transcriptional regulation of gene expression, including alternative pre-mRNA splicing, has emerged as an important means of control during neuronal morphogenesis. A suite of functionally conserved RNA-binding proteins with post-transcriptional roles in *Drosophila melanogaster* and *C. elegans* sensory neuron dendrite patterning have since been identified. Among these proteins are the Muscleblind splicing factors MBL/MBL-1, which have human homologs MBNL1-3 that are associated with myotonic dystrophy. Here we show that loss of *C. elegans mbl-1* function produces an aberrant PVD sensory neuron dendritic arbor, characterized by reduced dendrite terminal branching that becomes more severe with increasing distance from the neuronal cell body. We tested whether similar defects would be apparent for other types of *C. elegans* sensory neurons and confirmed the previous findings that the P/ALM and P/AVM gentle touch receptors exhibit truncated axons, and that the PLM synapse is positioned abnormally close to the cell body. We add the finding that the PLM dendrite is elongated in the *mbl-1* mutant. To test whether *mbl-1* function is required within muscle or within the nervous system to regulate PVD terminal dendrite patterning, we co-expressed muscle and PVD reporters within the same transgenic line to observe the muscle/PVD interface. We show that, beyond the reduction in terminal branches, loss of *mbl-1* function does not affect the stereotyped patterning of PVD muscle-skin interface innervation, and no defects in the macrostructure of the body wall muscle were evident in the mutant. Work from other labs has shown that *mbl-1* mutants fail to localize pre-synaptic proteins in the distal axon while excluding these components from the dendrite in some neuron types. Ongoing work in the lab seeks to test whether the PVD neuron displays a similar synaptic protein trafficking defect by expressing mCherry-tagged RAB-3 in the PVD neuron and monitoring its subcellular localization. Previous findings indicate that *mbl-1* might regulate PLM axon outgrowth by influencing the stability of *mec-7* (β-tubulin) and *mec-12* (α-tubulin) mRNA. We are testing whether decreased MEC-7 expression upon loss of *mbl-1* function might contribute to the dendrite patterning defect observed in the PVD neuron by overexpressing *mec-7* using a PVD-specific promoter. MBL-1 is predicted to function as a regulator of alternative splicing; to learn more about how defects in splicing may lead to neuron morphological changes, we aim to identify the direct mRNA targets of MBL-1 binding/regulation using ribonucleoprotein (RNP) immunoprecipitation followed by RNA sequencing. The identity and function of these targets may offer insights into the post-transcriptional mechanisms that regulate neuron morphogenesis.

Keywords: *Caenorhabditis elegans*; PVD neurons; dendrite morphogenesis; post-transcriptional regulation; RNA-binding proteins; alternative splicing; muscleblind-1

INTRODUCTION

Neuron Morphology and Function

Neurons are cells of the nervous system that are responsible for receiving, integrating, and transmitting sensory or synaptic information. Combining such diverse functions within a single cell that can then integrate into a functional neural circuit requires the segregation of neuronal processes into morphologically distinct compartments and the polarization of the overall neuronal architecture such that information is processed and transmitted unidirectionally. The dendrite, cell body, and axon are molecularly distinct neuronal compartments that receive, integrate, and transmit information, respectively. Within this compartmentalized organization, neurons can display diverse, and often highly-complex, morphologies. This structural variability affords functional versatility in the nervous system; neuron type-specific modes of information reception, processing, and communication provide the functional diversity necessary for neural circuits to perform complex computations and mediate sophisticated behaviors (Ledda and Paratcha, 2017).

Dendrites receive stimuli from the environment, in the case of sensory neurons, or from pre-synaptic neurons, in the case of interneurons and motor neurons. The morphology of the dendritic tree determines the size and shape of the neuron's receptive field and has important implications for the types of signals a neuron can receive (Jan and Jan, 2010). Nociceptive neurons in the fly and worm, which are sensitive to noxious mechanical stimuli and temperatures, elaborate extensively branched dendritic arbors that lie directly beneath the epidermis (Albeg et al., 2010; Grueber et al., 2002; Hwang et al., 2007). Pyramidal neurons in the mammalian neocortex extend large highly branched dendritic structures that contact numerous excitatory and inhibitory pre-synaptic targets (Ledda and Paratcha, 2017). The *C. elegans* PLM touch receptor neuron, which responds to gentle mechanical stimuli, projects a short unbranched dendritic process into the tip of the nematode tail, and the *C. elegans* proprioceptive PVD neuron extends thin finger-like projections that traverse the body wall muscle and respond to muscle tension (Albeg et al., 2010; Huang et al., 1995). Aberrant dendritic arbor morphology is associated with a host of human neurodevelopmental and neuropsychiatric disorders such as autism, Rett syndrome, schizophrenia, Alzheimer disease, Fragile X syndrome, Down syndrome, and bipolar disorders. Alterations in dendritic arbor size and spine density, in particular, have been found to contribute to the neuropathogenesis of these disorders (Kulkarni and Firestein, 2012). Given the well-established etiology of these myriad of human neurological conditions in disrupted neuron morphogenesis, it is important to understand the molecular genetic mechanisms that give rise to these structures.

Mechanisms of Neuronal Morphogenesis: Transcriptional Regulatory Cascades

The combinatorial activity of a large array of intrinsic and extrinsic cues regulates neuronal morphogenesis. Functioning as a primary intrinsic cue, transcription factors heavily influence neuronal identity and neuron type-specific dendrite patterning by regulating expression patterns for large collections of genes (Jan and Jan, 2010; Ledda and Paratcha, 2017). Certain transcription factors are known to function as master

regulators of cell identity; for example, the *D. melanogaster glial cells missing* (*gcm*) gene encodes a transcription factor that controls the decision between neuronal and glial fate by activating the transcriptional program that leads to glial differentiation. Downstream targets of *gcm* include other transcription factors that are capable of regulating their own gene complements. In this way, the role of *gcm* can be described as the initiator of a genetic cascade that eventually engages all of the genetic components required to build a glial cell from an undifferentiated precursor (Egger et al., 2002). Downstream of these master regulators of cell identity, transcription factors function to define specific aspects of neuronal morphogenesis and type-specific neuronal morphologies can be achieved by adjusting the expression of a single transcription factor or through the combinatorial effects of many transcription factors. For instance, a handful of conserved transcription factors have been identified which function cell autonomously within the *D. melanogaster* larval dendritic arborization (da) neurons to coordinate the size and branching complexity of the dendritic arbor (Jan and Jan, 2010). Another example of an important transcription factor for neuron development is *C. elegans* FOXO which is critical for the establishment of neuronal polarity. Knockdown of *C. elegans* FOXO results in axon outgrowth defects combined with dendritic overgrowth, signifying the loss of neurite identity (Christensen et al., 2011; Ledda and Paratcha, 2017). Many of these transcription factors have homologs in mammals which have been shown to contribute to CNS development. For instance, human *Cux2*, a homolog of the *D. melanogaster* CUT homeodomain transcription factor, has been implicated in several human neurodevelopmental disorders (Barington et al., 2018; Cubelos et al., 2010; Kulkarni and Firestein, 2012).

Mechanisms of Neuronal Morphogenesis: Receptors

The *D. melanogaster* Down syndrome cell adhesion molecule (DSCAM) functions as an extrinsic cue to mediate dendrite self-avoidance and the co-existence of functionally distinct neurons. Sister dendrite self-avoidance and tiling of dendritic arbors established by neurons of the same type or function are important features of dendritic morphogenesis that enable efficient and unambiguous coverage of the receptive field. Extensive alternative splicing of *Dscam* provides each neuron in the *D. melanogaster* nervous system with a unique zip code consisting of a small subset of stochastically expressed DSCAM isoforms. Neuronal identity mediated through DSCAM enables neurite self-recognition and contact-dependent self-avoidance (Jan and Jan, 2010; Ledda and Paratcha, 2017). Many additional transmembrane receptors and their associated ligands function within the nervous system to regulate aspects of neuronal development such as self-avoidance and directional growth. Cell-cell communication mediated by these receptor-ligand pairs allows neurons to respond to their extracellular environments which is a necessary feature of developmental processes such as axon guidance and the targeting of dendrites to their appropriate receptive fields (Jan and Jan, 2010; Ledda and Paratcha, 2017). For example, the conserved netrin family of diffusible signaling molecules participates in commissural axon guidance in both vertebrates and invertebrates. These chemoattractant signaling proteins are produced by midline cells and help direct commissural axon outgrowth by forming a concentration gradient that is sensed by their cognate DCC family receptors in the axon growth cone. The Slit family of chemorepellent signaling molecules ensures that commissural axons

do not remain at or recross the midline by blocking attractive netrin signaling after the initial crossing through a direct physical interaction between the Slit cognate receptor Robo and DCC, which interferes with the ability of the DCC receptor to transmit signals from netrin across the cell membrane (Stein and Tessier-Lavigne, 2001).

Mechanisms of Neuronal Morphogenesis: Regulators of Cytoskeletal Organization and Motor Protein Behavior

Downstream of transcription factors and receptors, neuron morphology is ultimately a product of cytoskeletal dynamics and motor protein behavior. The highly polarized and compartmentalized organization of the neuron requires tightly regulated mechanisms for the polarized transport and sorting of subcellular cargoes. Robust targeting of axonal/dendritic cargoes to the appropriate subcellular compartments requires the polarization of the microtubule cytoskeleton and the regulation of polarized motor-based transport through mechanisms that modulate motor activity and cargo binding such as post-translational modification of cytoskeletal components and motor-cargo adaptors and accessory proteins. Microtubules are polymerized from α-tubulin and β-tubulin heterodimers, displaying an inherent polarity with molecularly distinct plus and minus ends (Kapitein and Hoogenraad, 2011). Within invertebrate neurons, microtubules are organized into uniformly oriented bundles that populate neurites, such that, for example, the *C. elegans* bipolar DA9 motor neuron exhibits plus-end-out oriented microtubule architecture within its axon and minus-end-out oriented microtubule architecture within its dendrite (Kapitein and Hoogenraad, 2011; Yan et al., 2013). This DA9 microtubule organization appears to be fairly generalizable to the rest of the *C. elegans* nervous system (Rolls, 2022). Conversely, vertebrate neurons have been shown to enrich plus-end-out microtubules within their axons, while maintaining a mixed microtubule orientation within their dendrites (Kapitein and Hoogenraad, 2011).

Uncoordination, or abnormal locomotion, is a common phenotype observed in *C. elegans* resulting primarily from genetic mutations that affect neuron or muscle function. Behaviors associated with the unc phenotype include twitching, curling, halting, and paralysis, among others (Herndon et al., 2013). In the *C. elegans* DA9 motor neuron and PHC sensory neuron, *unc-116* (kinesin-1/kinesin heavy chain), a plus-end-directed microtubule motor protein, has been shown to mediate the polarization of the dendrite microtubule cytoskeleton by cross-linking anti-parallel microtubules and sliding the plus-end-out oriented microtubules out of the dendrite through the activation of its motor domain. In the absence of *unc-116*, DA9 and PHC dendrites become more axon-like; their microtubule polarity becomes plus-end-out oriented, and dendrites fail to accumulate post-synaptic proteins while becoming enriched in mislocalized pre-synaptic components. These findings suggest that polarization of the neuronal cytoskeleton is necessary for the directed transport, sorting, and compartmentalization of subcellular cargoes (Yan et al., 2013).

Motor-cargo adaptor proteins have also been shown to play important roles in nervous system development and maintenance. The conserved *C. elegans* UNC-76 protein is a predicted UNC-116 (Kinesin-1) adaptor that is required for proper axon outgrowth, fasciculation, and synaptic organization. There is evidence that UNC-76 mediates these processes through its interaction with UNC-116 and by influencing axonal transport, but

it remains to be clarified whether UNC-116 provides additional regulation of UNC-116 motor activity or facilitates trafficking of an alternative set of UNC-116 cargoes (Su et al., 2006; Sure et al., 2018). Su *et al.* (2006) propose a model where UNC-69 and UNC-76 form a protein complex that functions downstream of axon guidance and outgrowth cues to regulate the delivery of phospholipid-containing vesicles derived from the Golgi apparatus to the plasma membrane of the extending growth cone. In UNC-76 mutants, ectopic branches extend from the cell body while the axon growth cone fails to reach its target, suggesting that the UNC-69/UNC-76 protein complex restricts the addition of new membrane to the developing growth cone (Su et al., 2006; Ye et al., 2006). In summary, the complex structure of a neuron and its resultant functionality is a product of the neuron's cytoskeletal organization and ability to localize machinery within distinct subcellular compartments.

The *C. elegans* PVD Neurons as a Model for the Genetic Regulation of Dendrite Development

The *C. elegans* hermaphrodite nervous system consists of 302 highly stereotyped neurons (out of 959 total somatic cells in the adult hermaphrodite) organized into ganglia in the head and tail (Figure 1). Axon fascicles extend along internal hypodermal ridges, forming the major ventral and dorsal nerve cords, as well as the peripheral lateral and sublateral nerve cords. Despite being the most complex organ in the nematode, the invariant anatomy and relative simplicity of the *C. elegans* nervous system have allowed it to be described in unprecedented detail based on electron microscopy (EM) reconstructions (Altun et al., 2024; Cook et al., 2019; White et al., 1986).

Almost all *C. elegans* neurons display simple morphologies with mostly unbranched processes (Altun et al., 2024; Cook et al., 2019; White et al., 1986). The striking exception to this rule is the two *C. elegans* PVD and FLP sensory neurons which elaborate large highly branched dendritic structures that innervate the skin (Albeg et al., 2010; Smith et al., 2010). The PVD and FLP neurons are excellent models for studying dendrite development and patterning due to their complex and highly ordered morphologies in an organism that is amenable to genetic manipulation and live imaging. Live imaging is facilitated by the fact that nematodes are transparent at all life stages. The PVD and FLP neurons have similar morphologies and sensory modalities, and their dendritic arbors are tiled, with the PVD neurons enveloping the body of the worm and the FLP neurons enveloping the head, to provide complete and unambiguous sensory coverage of the entire epidermis (Albeg et al., 2010; Chatzigeorgiou et al., 2010; Liu et al., 2012; Smith et al., 2010). The PVD and FLP neurons are polymodal nociceptors that respond to high threshold mechanical stimuli and noxious temperatures, with the PVD sensing extreme cold and the FLP sensing extreme heat (Chatzigeorgiou et al., 2010; Liu et al., 2012). These neurons mediate an escape behavior upon activation by noxious stimuli consisting of increased forward crawling speed and reduced reversals. The PVD neurons have also been reported to function as proprioceptors, as ablation of the PVD cell bodies leads to defects in posture and aberrant sinusoidal waveforms during forward movement. This function is likely mediated by the PVD's thin finger-like terminal branches that extend over the body wall muscle and respond to body bending (Albeg et al., 2010).

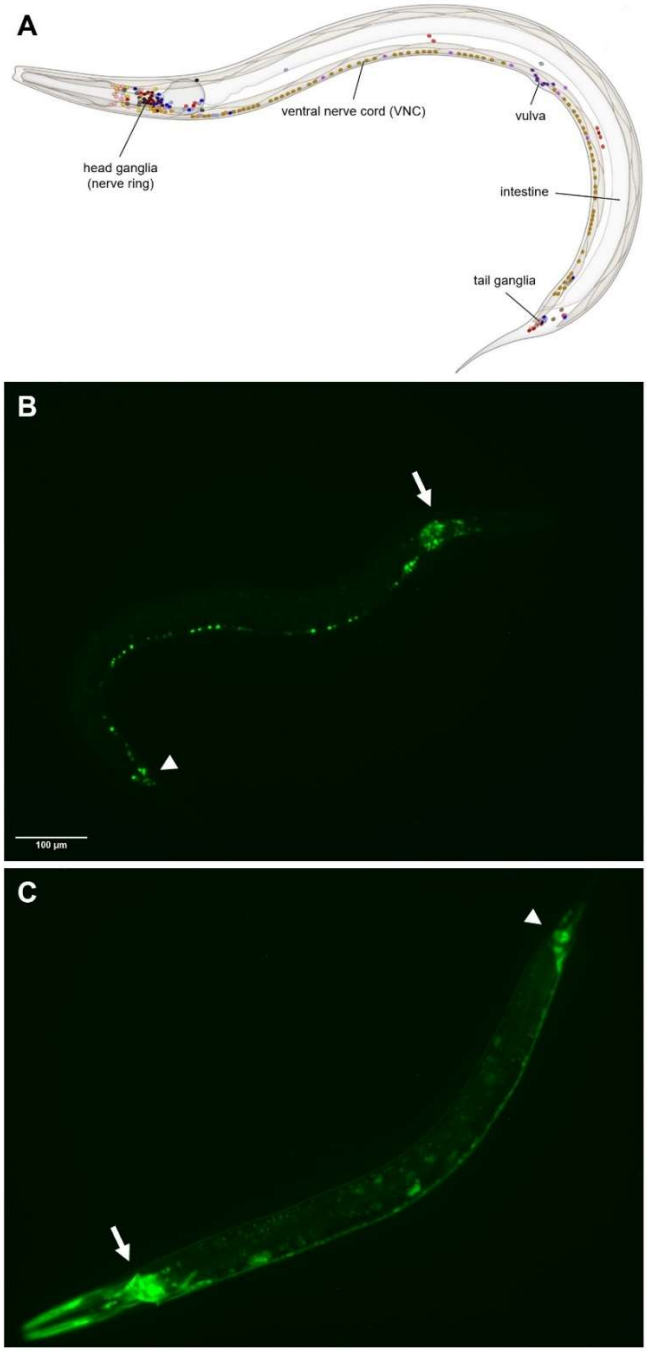

Fig 1. Structure of the *C. elegans* hermaphrodite nervous system. (A) Schematic representation of *C. elegans* neuroanatomy. Modified from Cook et al. (2019). (B, C) A transgene expressing nuclear MBL-1::GFP (B) and cytoplasmic GFP (C) throughout the *C. elegans* nervous system under the control of the pan-neuronal *rab-3* promoter. Neuronal cell bodies are organized into ganglia in the nematode head (arrows) and tail (arrowheads). The ventral nerve cord (VNC) is the major axon tract which runs along the length of the body. The VNC is homologous to the vertebrate spinal cord.

The two *C. elegans* PVD neurons are born post-embryonically and their cell bodies occupy posterior lateral positions on the left (PVDL) and right (PVDR) sides of the worm (Figure 2). During the L2 larval stage, the PVD cell bodies elaborate bilateral first-order (1°) dendritic processes that extend anteriorly and posteriorly and co-localize with the lateral nerve cord. The anterior border of the PVD dendritic arbor is defined by the FLP neuron, which forms a non-overlapping dendritic tree in the head of the worm. During the L2 larval stage, the PVD neuron also extends a ventral process that forms presynaptic contacts with neurons of the ventral nerve cord. During the L3 larval stage,

second-order (2°) dendritic branches emerge from the 1° process and extend orthogonally towards the dorsal and ventral sublateral nerve cords. 2° branch elaboration consists of dynamic branch growth and retraction, with nascent 2° processes sometimes withdrawing completely back into the 1° branch. This dynamic process of branch extension and retraction produces a stereotyped number of mature evenly spaced 2° branches by the end of the L3 larval stage. While most 2° branches do not fasciculate with motor neuron commissures, evidence suggests that commissural motor neuron processes can act as landmarks for 2° branch extension towards the sublateral nerve cord (Albeg et al., 2010; Smith et al., 2010).

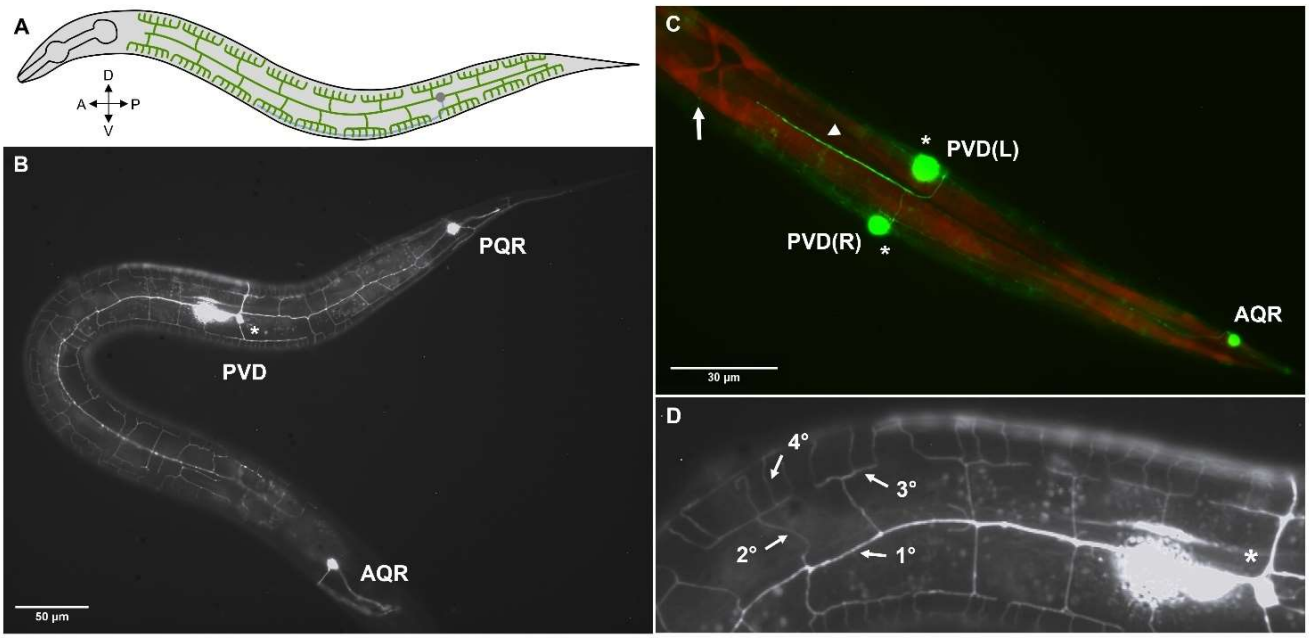

Fig 2. The *C. elegans* PVD sensory neurons elaborate highly branched dendritic arbors. (A) Schematic of PVD neuron morphology. The lateral PVD cell body (grey) extends a single axon (blue) towards the VNC. Upon reaching the midline, the PVD axon fasciculates with the nerve cord and projects anteriorly towards the head. The PVD dendritic arbor (green) innervates the nematode epidermis, forming a non-overlapping sensory field that extends from the tail to the pharynx. (B) Epifluorescence micrograph of the PVD(L) neuron showing the neuronal cell body (asterisk) and the dendritic arbor. PVD morphology was visualized using the transgenic marker *wdIs52* ($P_{F49H12.4}$::GFP), which also labels the P/AQR sensory neurons in the head and tail. (C) Epifluorescence micrograph of an animal co-expressing $P_{F49H12.4}$::GFP (PVD; green) and P_{myo-3}::mCherry (body wall muscle; red). Ventral view of the PVD neurons shows the lateral cell bodies (asterisks) and the two unbranched PVD axons (arrowhead) which terminate prior to reaching the vulva (arrow). Fourth-order (4°) PVD dendritic projections grow towards the midline between the epidermis and the underlying body wall muscle. (D) The PVD dendritic arbor forms a series of candelabra-like structures composed of 2° (stems), 3° (bases), and 4° (candles) branches.

During the late L3 and early L4 stages, mature 2° branches turn 90° to form an orthogonal branch that tracks the sublateral nerve cord. The majority of these “L” shape structures eventually bifurcate to form a collateral third-order (3°) branch that projects both anteriorly and posteriorly along the sublateral line. To ensure complete coverage of the receptive field and a non-overlapping dendritic arbor, 3° branches frequently extend along the A/P axis until they come into contact with an adjacent 3° branch, at which point, mechanisms of contact-dependent self-avoidance, mediated by the transcription factors *atf-2* and *thoc-2*, trigger the developing 3° branches to retract slightly and

stabilize. In the final stage of PVD development, fourth-order (4°) dendritic branches originate at periodic intervals along the stabilized 3° branches and project between the body wall muscle and the epidermis towards the ventral or dorsal midlines. 4° branches display dynamic growth and are usually stabilized by the young adult stage. The completed PVD dendrite structure is often described based on its resemblance to a series of 'candelabras' composed of 2° (stems), 3° (bases), and 4° (candles) branches (Figure 2D). Higher-order PVD branches (5°, 6°) have also been observed to form from some 4° branches. Terminal branching encompasses both the 4° parent branch and any higher-order branches that originate from it (Albeg et al., 2010; Smith et al., 2010).

Deviations in the highly stereotyped patterning of the PVD dendritic arbor are easily identifiable, conferring efficiency and reproducibility to genetic screens that utilize this neuron. Furthermore, by incorporating time-lapse imaging of PVD development into these screens, molecular factors involved in dendrite patterning can be further characterized based on the specific morphogenetic processes that they regulate. Smith *et al.* (2010) used this approach to show that the homeodomain transcription factor MEC-3 is required in the PVD neuron for 2° branch initiation during early larval development. Using time-lapse analysis, Dong *et al.* (2013) identified *sax-7*, *mnr-1*, and *dma-1* as necessary factors for 3° branch initiation and stabilization. Due to the similar nature of these genes' involvement in PVD dendrite patterning, Dong *et al.* (2013) hypothesized that they might function within the same genetic pathway. SAX-7 and MNR-1 were shown to be necessary within the epidermis for proper PVD morphogenesis, while DMA-1 was shown to be necessary within the PVD neuron itself. While MNR-1 is not subcellularly localized within the hypodermal cell, a SAX-7::GFP (green fluorescent protein) translational reporter revealed subcellular enrichment of SAX-7 in lateral and sublateral stripes that co-localize with PVD 1° and 3° dendritic branches. By ectopically expressing SAX-7 and MNR-1 together in sublateral cord neurons and motor neuron commissures, Dong *et al.* (2013) were able to partially rescue the PVD phenotype associated with the *sax-7*; *mnr-1* double mutant, and using a *Drosophila* S2 cell aggregation assay, they demonstrated a physical interaction between SAX-7, MNR-1, and DMA-1 that only occurred when cells were co-transfected with SAX-7 and MNR-1. These findings suggest that SAX-7 and MNR-1 function together as co-ligands in the hypodermal cell and DMA-1 functions as the cognate receptor in the PVD neuron. Dong *et al.* (2013) propose a model where SAX-7 acts as a pre-patterned guidance cue in the hypodermal cell to instruct PVD dendrite patterning. One possibility is that SAX-7 and MNR-1 mediate 3° dendrite initiation by signaling through the DMA-1 receptor to recruit downstream cytoskeletal components to the site of branch formation. SAX-7, MNR-1, and DMA-1 also function as membrane adhesion molecules, likely anchoring developing 3° branches to the hypodermal cell and limiting their retraction. Loss of adhesion in the *sax-7*, *mnr-1*, and *dma-1* mutants might explain the observed 3° branch stabilization defect. Hence, the dual functionality of the tripartite ligand-receptor complex, with signaling and adhesion cooperating to produce mature properly positioned branches, suggests a method of error correction during dendrite morphogenesis (Dong et al., 2013). Overall, these findings highlight the importance of the growth substrate during PVD dendrite development, both as a source of extrinsic

signaling molecules to direct outgrowth and extracellular anchors to stabilize nascent branches.

To conclude, the *C. elegans* PVD sensory neurons are an excellent system for studying dendrite patterning due to their morphological complexity and structural similarity to mammalian nociceptors in an otherwise simple and accessible invertebrate model organism (Albeg et al., 2010; Smith et al., 2010). While several molecular genetic factors that contribute to the morphogenesis of this neuron type have been described in detail, much remains to be learned especially in regard to the genes downstream of transcription factors and receptors that mediate the actual mechanical changes to PVD shape. At a most basic level, neuron morphology is a product of cytoskeletal dynamics and presently several cytoskeleton-associated proteins including *unc-116* (kinesin-1/kinesin heavy chain) and *dli-1* (dynein light intermediate chain) are known to contribute to dendrite pattern formation in the PVD neuron (Aguirre-Chen et al., 2011; Tang and Jin, 2018). However, a relevant open question is whether the genetic pathways that regulate neuron morphogenesis utilize intermediary proteins that are involved in the integration, modification, and transmission of signals on their way from upstream transcription factors and receptors to the downstream cytoskeleton-associated proteins which are ultimately responsible for enacting changes to neuron shape. Recent evidence points to post-transcriptional gene regulation mediated by RNA-binding proteins as a possible mechanism by which cytoskeleton-associated protein behavior could be fine-tuned and rapidly adjusted in response to changing intrinsic and extrinsic signals (Albeg et al., 2010; Antonacci et al., 2015; Dong et al., 2013; Olesnicky et al., 2018, 2014; Olesnicky and Killian, 2020; Schachtner et al., 2015; Sharifnia et al., 2015; Smith et al., 2010).

An Emerging Mechanism of Neuronal Morphogenesis: Post-Transcriptional Gene Regulation Mediated by RNA-Binding Proteins

Recent studies have emphasized the importance of post-transcriptional gene regulation mediated by RNA-binding proteins (RBPs) and translation factors during nervous system development. The *C. elegans* and *D. melanogaster* genomes both encode several hundred RBPs, many of which are conserved across diverse metazoan phyla and have been shown to function in the mammalian central nervous system (Antonacci et al., 2015; Olesnicky et al., 2018, 2014; Sharifnia et al., 2015). Given the elaborate cellular morphologies that characterize the nervous system, this outsized reliance on post-transcriptional regulatory mechanisms is frequently explained by a need for fast localized decision-making within distal neuronal and glial processes that can be far removed from the site of transcriptional control in the cell body. However, while mechanisms of transcriptional regulation in the developing nervous system have been extensively characterized in many organisms, the guiding principles and molecular mechanisms underlying post-transcriptional control of neuronal morphogenesis remain understudied (Sharifnia et al., 2015).

Through a candidate genetic screen, Antonacci *et al.* (2015) identified a conserved suite of 12 *C. elegans* RBP-encoding genes with functions in sensory neuron dendrite patterning. Homologs for all twelve of these RBP-encoding genes were previously shown to be important for dendrite morphogenesis in the *D. melanogaster* larval class

IV da sensory neurons (Olesnicky et al., 2014). The functional conservation of this set of RBPs emphasizes the importance of mRNA regulation in neuronal development (Antonacci et al., 2015; Olesnicky et al., 2014). Loss or reduction of RBP gene function revealed a decrease in dendritic terminal branching of the PVD multidendritic sensory neurons. Importantly, the finding that these 12 genes are expressed in the PVD neuron supports the cell-autonomous function of some or all of these RBPs in dendrite patterning (Antonacci et al., 2015). Interestingly, loss-of-function alleles for two of the RBP-encoding genes, *cgh-1* and *cpb-3*, identified in this study revealed an increase in 2° and 3° PVD dendritic branching concomitant with a reduction in dendritic termini (Antonacci et al., 2015). CGH-1 and CPB-3 influence translational repression/activation of target mRNAs and have been shown to localize to motile particles within the PVD dendritic arbor, suggesting a possible role during microtubule-based mRNA transport (Pimentel et al., 2014; Rajyaguru and Parker, 2009; Spendier et al., 2021; Villalba et al., 2011). The perinuclear enrichment of CGH-1 within the PVD neuron and its localization to motile dendritic puncta support a model where CGH-1 binds to newly transcribed mRNA molecules in the cell body and suppresses their translation as they are targeted to the dendritic compartment by other components of the ribonucleoprotein (RNP) complex (Antonacci et al., 2015; Spendier et al., 2021). Alternatively, CGH-1 might play an active role in mRNA transport or localization. Therefore, CGH-1 and CPB-3 target mRNAs may be prematurely translated in the respective mutant animals due to a defect in translational repression and/or transport, leading to an increase in lower-order dendritic branches at the expense of terminal branching (Antonacci et al., 2015; Spendier et al., 2021).

RNAi-mediated knockdown of conserved RBP-encoding genes in *D. melanogaster* affected changes in dendritic branch number, branch length, and branch patterning. In addition, extensive terminal branch clustering was observed for many of the RBP genes, consistent with a defect in sister dendrite self-avoidance. Regardless of the specific nature of the dendrite organization defect, gaps in receptive field coverage occurred ubiquitously for all RBP-encoding genes analyzed in this study (Olesnicky et al., 2014). Therefore, post-transcriptional gene regulation mediated by these genes is clearly important for sensory neuron function. Knockdown of *muscleblind* (*mbl*) and *x16* gene function resulted in an increase in class IV da neuron dendrite branch points and a concomitant decrease in total dendrite length, such that the ratio of branch number to arbor size was significantly elevated (Olesnicky et al., 2014). Conversely, loss of the *C. elegans* X16 homolog RSP-6 was associated with fewer PVD dendritic termini, while loss of the *C. elegans* Muscleblind homolog MBL-1 caused a reduction in branching at all orders (Antonacci et al., 2015). Since both of these genes are predicted to encode splicing factors, this phenotypic analysis suggests a role for alternative splicing in the determination of dendritic branch number, although Mbl/MBL-1 and X16/RSP-6 may influence this morphogenetic process differently in *C. elegans* and *D. melanogaster*.

Overall, six of the twelve RBP-encoding genes identified in the *C. elegans* screen are predicted or known to function as alternative splicing regulators (Antonacci et al., 2015). This suggests that alternative splicing plays a widespread role in dendrite development. For instance, specific protein isoforms might contribute to dendrite patterning, while other protein isoforms from the same gene do not. Alternatively, protein isoforms may

function antagonistically to one another such that the relative amount of each isoform regulates some aspect of dendrite architecture. In addition, alternative splicing can influence the localization, stability, and/or translation rate of mRNA molecules by mediating alternative 5'- or 3'-untranslated region (UTR) usage. While differential 5'- and 3'-UTR usage coordinated by splicing factors does not impact an mRNA's coding sequence, it does impact how other post-transcriptional regulatory factors interact with the transcript and mediate its downstream processing. Likely, the combinatorial activity of large networks of alternatively spliced genes determines neuron cell fate and type-specific dendrite morphogenesis, where differences in the activity of alternative splicing factors between cell types produce subtle differences in mRNA isoform production for many genes, which, in combination, generates the large repertoire of dendrite morphologies found in the nervous system (Baralle and Giudice, 2017).

In the *Drosophila* RNAi screen, the most severe dendrite defects were observed upon loss of translation initiation factors, including *eIF-1A* and several *eIF-2* and *eIF-3* subunits (Olesnicky et al., 2014). This role for general translation factors in neuronal development may reflect the heightened need for local translation within the dendritic arbor and the axon growth cone. In mammals, zipcode binding protein 1 (ZBP1) demonstrates the possibility for direct interaction between RNA-binding proteins and components of the neuronal cytoskeleton. By regulating the transport and local translation of β-actin mRNA in the axon growth cone, ZBP1 stimulates filopodia and lamellipodia growth in the direction of secreted guidance molecules (Welshhans and Bassell, 2011). In summary, post-transcriptional mechanisms such as alternative mRNA splicing, mRNA transport and localization, mRNA stability, and translational control are important contributors to neuronal morphogenesis in diverse animal species.

Molecular Functions of MBNL Family Proteins in Model Systems

The Muscleblind-like protein family (MBNL) is an evolutionarily conserved family of tandem CCCH-type zinc finger motif-containing RNA-binding proteins that function as regulators of alternative splicing (Figure 3; Pascual et al., 2006). The *D. melanogaster muscleblind* (*mbl*) gene was the first MBNL family homolog characterized for its role in the terminal differentiation of photoreceptors and muscle cells. *mbl* mutants exhibit a lethal phenotype with partial paralysis and blindness in the first instar larval stage. Hence, the Muscleblind-like protein family derives its name from the established function of *D. melanogaster mbl* in the fly somatic musculature and eye (Artero et al., 1998; Begemann et al., 1997). In humans, the sequestration of MBNL protein by expanded CUG-repeats in the 3'-UTR of the *dystrophia myotonica protein kinase* (*DMPK*) transcript leads to the neuromuscular disease myotonic dystrophy type 1 (DM1) as a result of defects in the alternative splicing of MBNL target genes. DM1 is characterized by muscle degeneration, cataracts, and neurological symptoms including cognitive impairment and behavioral abnormalities (De León and Cisneros Vega, 2008; Lee and Cooper, 2009). This indicates that Muscleblind-like protein family homologs function in the central nervous system (CNS) and muscle tissue in organisms as distinct as fly and humans, a proposition that is further supported by data from the Genotype-Tissue Expression (GTEx) project that shows enrichment of human MBNL2 in the brain and spinal cord (Lonsdale et al., 2013; Pascual et al., 2006).

In contrast to the three paralogous MBNL genes (*MBNL1-3*) present in the human genome, the *C. elegans* genome encodes only one MBNL homolog, *mbl-1*, which functions extensively within the nematode peripheral nervous system to regulate neuronal development (Pascual et al., 2006; Sasagawa et al., 2009). The *mbl-1* gene is required cell autonomously in the excitatory DA9 motor neuron for proper neuromuscular junction (NJM) synapse formation. Interestingly, *mbl-1* also regulates the patterning of DA9 synapses along the dorsal nerve cord, as loss of *mbl-1* function selectively eliminates only the most distal NJM synapses. In wild-type DA9 motor neurons, synaptic vesicle-associated RAB-3 and active zone proteins UNC-10 and SYD-2 co-localize as puncta in the motoneuron axon at the sites of NJM synapses. Conversely, these pre-synaptic proteins are largely excluded from the DA9 dendrite. In *mbl-1* mutant animals, GFP::RAB-3, UNC-10::GFP, and GFP::SYD-2 puncta were missing from the distal DA9 axon, revealing the defect in NJM synapse formation. Concurrently, GFP::RAB-3 puncta became visible in the DA9 dendrite, signifying a defect in axonal targeting of pre-synaptic components and/or dendritic exclusion of these molecules. The DA motoneurons innervate dorsal body wall muscle and are involved in backward locomotion. *mbl-1* function is required for this behavior and mutant worms abnormally curve ventrally during backing, signaling a reduction in dorsal muscle activation. This provides strong evidence that *mbl-1* is functionally important within the nematode peripheral nervous system (Spilker et al., 2012).

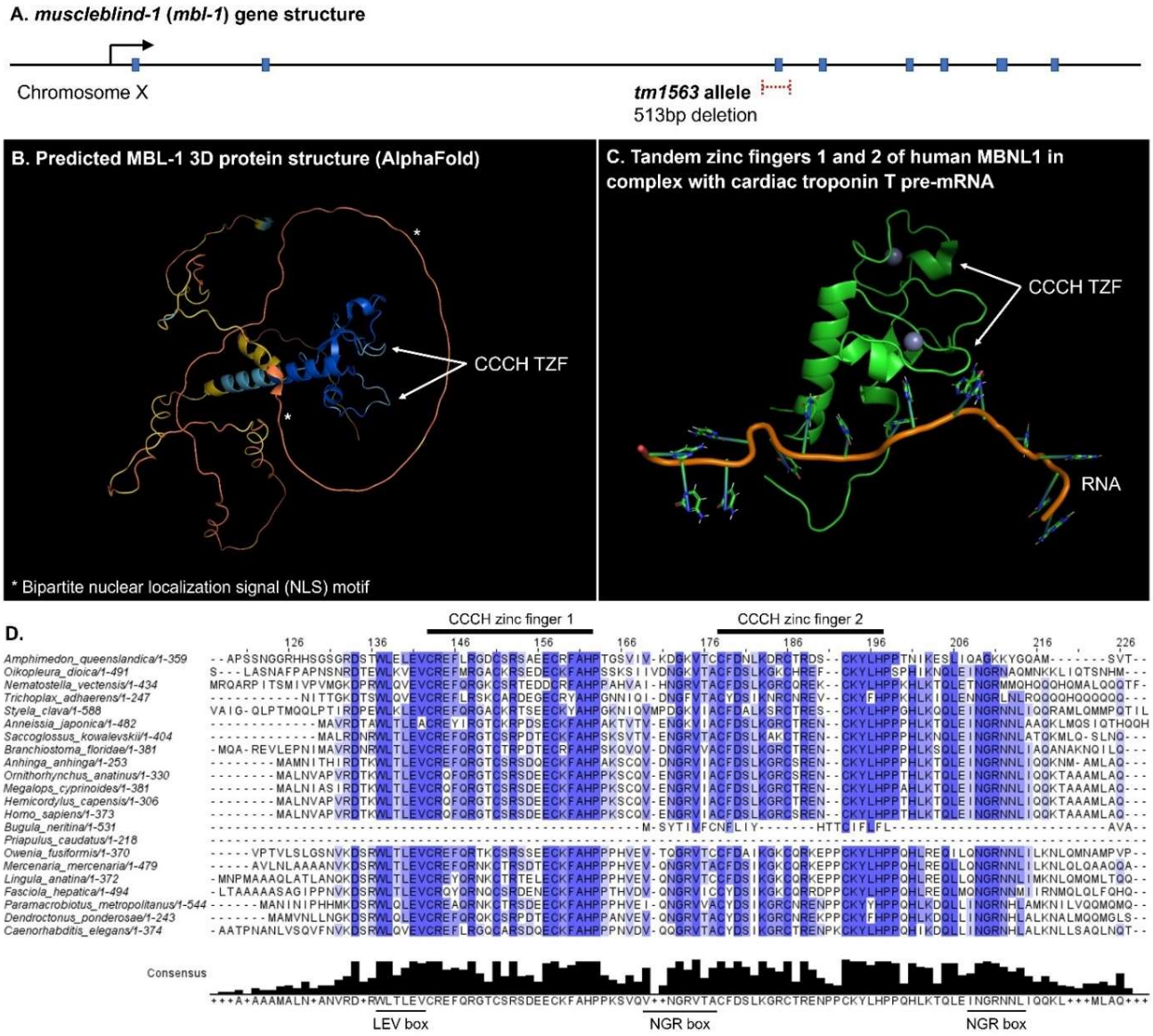

Fig 3. *mbl-1* encodes an evolutionarily conserved regulator of alternative splicing predicted to bind pre-mRNA through its tandem CCCH zinc finger domain. (A) The *C. elegans mbl-1* gene is located on chromosome X. In this schematic diagram of *mbl-1* gene structure, exons are represented by blue boxes connected by horizontal black lines representing introns. Alternative splicing of the *mbl-1* transcript produces several distinct MBL-1 protein isoforms with specialized functions in RNA metabolism (Verbeeren et al., 2023). The *mbl-1(tm1563)* allele contains a large deletion which includes the entirety of exon 3 and adjacent intronic sequences. *mbl-1(tm1563)* is a putative null allele due to a predicted frameshift and the introduction of an early stop codon such that a severely truncated gene product is produced. (B) *In silico* MBL-1 3D protein structure prediction by AlphaFold (Jumper et al., 2021) with the locations of the CCCH tandem zinc finger (TZF) domain and bipartite KR (lysine-arginine) motif nuclear localization signal (NLS; asterisks) highlighted. The MBL-1 bipartite NLS is partially encoded by exon 7 and partially encoded by exon 8, such that the short (exon 7 excluded) isoform of MBL-1 has an interrupted version of the NLS sequence and displays a diffuse pattern of nuclear and cytoplasmic localization (Verbeeren et al., 2023). Color coding reflects the

confidence score of the predictive AlphaFold model (dark blue: very high; light blue: confident; yellow: low; orange: very low). (C) Solved 3D structure of human MBNL1 in complex with cardiac troponin T pre-mRNA (only the two TZF motifs and adjacent regions are shown here). The CCCH zinc finger structural motifs encoded by MBNL family proteins (e.g., CeMBL-1 and HsMBNL1) coordinate positively charged zinc ions (Zn^{2+}) which are essential for the binding of pre-mRNA molecules (Park et al., 2017; Pascual et al., 2008). The sequence specificity of RNA binding by MBNL proteins is mediated by amino acid residues that interact with nucleotide bases in the RNA molecule and lower the binding energy for specific RNA sequence motifs (e.g., 5'-CHG-3' and 5'-CHHG-3' for HsMBNL1 where H is A, U, or C; (Park et al., 2017; Pascual et al., 2008). (D) Amino acid sequence alignment within the first tandem CCCH zinc finger domain from diverse metazoan species across the Animalia kingdom, including *C. elegans* (*mbl-1*) and *Homo sapiens* (*MBNL2*). Within this region, Muscleblind family proteins show several highly conserved sequence motifs including the two CCCH zinc fingers, a LEV box (consensus sequence: WLXLEV where X indicates any amino acid) which directly proceeds the first CCCH zinc finger, and two NGR boxes (consensus sequence: $V/IX_{0-2}NGRV/NXA/L$) which flank the second CCCH zinc finger (Pascual et al., 2008). Muscleblind is suspected to have arisen early in metazoan evolution as is evidenced by the identification of Muscleblind homologs in most metazoan phyla and its pronounced absence in the ctenophores, choanoflagellates, and all other non-animal eukaryotic and prokaryotic lineages (Pascual et al., 2006).

The alternatively spliced neuronal kinase *sad-1* has been identified as a direct target of MBL-1 protein (Thompson et al., 2019). *sad-1* encodes two isoforms which may regulate neuronal polarization and synaptic organization differently (Kim et al., 2010). While most *C. elegans* neurons express a mixture of both isoforms, the ALM mechanosensory neurons and the BDU interneurons are unique in that they only express the exon 15-included isoform or the exon 15-excluded isoform, respectively. Thompson *et al.* (2019) show that the transcription factors *unc-86*, *mec-3*, and *alr-1* trigger expression of two RBPs, *mbl-1* and *mec-8*, in the ALM neurons, while the BDU neurons do not express these genes. Both MBL-1 and MEC-8 bind to the intronic regions surrounding the alternatively spliced *sad-1* cassette exon (an intervening exon that can be either included or skipped during alternative splicing in order to generate two distinct protein isoforms) and mediate the inclusion of this exon. The combinatorial activity of both RBPs is required for complete exon inclusion in the ALM neurons, while loss of both RBPs results in a BDU neuron-like *sad-1* expression profile consisting of complete exon exclusion. Loss of only *mec-8* results in expression of both *sad-1* isoforms in the ALM neuron, suggesting that *mbl-1* mediates *sad-1* exon inclusion but is not entirely effective on its own at preventing exon skipping. Cholinergic motor neurons (identity not specified) of the anterior ventral nerve cord natively express both isoforms of *sad-1*. In these neurons, *mbl-1* is the sole RBP that regulates *sad-1* splicing. Conversely, within inhibitory GABAergic motor neurons of the ventral nerve cord, partial *sad-1* exon inclusion is mediated by the functionally related RBP MSI-1. In summary, the default *sad-1* splice pattern is complete exon exclusion, while a redundant set of RNA-binding proteins with neuron type-specific expression patterns interact physically with the *sad-1* transcript to induce expression of the exon-included isoform. This research provides evidence that *mbl-1* functions within the ALM mechanosensory neurons and the ventral cholinergic motor neurons to regulate alternative splicing of a gene involved in neuronal development (Thompson et al., 2019).

Puri *et al.* (2023) show that MBL-1 physically interacts with *sad-1* mRNA within the PLM mechanosensory neuron to regulate its splicing. Importantly, they also show that *mbl-1* and *sad-1* single mutants display a similar synaptic positioning defect in the PLM neuron where the synaptic branch to the ventral nerve cord is shifted closer to the PLM cell body. This synaptic phenotype recapitulates the excitatory DA9 motor neuron mutant phenotype characterized by loss of the distal-most NJM synapses (Spilker et al., 2012). *mbl-1; sad-1* double mutants do not display an exacerbated PLM phenotype and overexpression of the exon-included *sad-1* isoform in the PLM neuron in an *mbl-1* null background rescues the synaptic positioning defect. These findings are consistent with a model where *mbl-1* regulates synapse positioning within the PLM neuron through its effects on the alternative splicing of *sad-1* transcript. It is also possible that synapse formation and positioning defects in the DA9 motor neuron result from *mbl-1*-mediated defects in *sad-1* splicing. In this model, the relative amounts of the exon-included and the exon-excluded isoforms of *sad-1*, as specified by the activity of MBL-1 and other related RNA-binding proteins, regulate the linear position of the synapse(s) along the axonal process with respect to the cell body. Puri *et al.* (2023) show that anterograde transport of GFP::RAB-3 within the proximal PLM axon is reduced in the *mbl-1* mutant. Therefore, *sad-1* might exert its effects on synapse positioning by regulating the balance of anterograde and retrograde axonal transport of pre-synaptic components. In the wild-type PLM neuron, anterograde RAB-3 transport events far outnumbered retrograde transport events, whereas in the *mbl-1* mutant, anterograde and retrograde RAB-3 transport occurred at roughly equal rates. This could help explain why the mutant PLM neurons frequently form synapses within the immediate vicinity of the neuronal cell body (Puri et al., 2023; Spilker et al., 2012).

Puri *et al.* (2023) also demonstrated a physical interaction between MBL-1 and *mec-7* and *mec-12* mRNA within the PLM neuron using RNP immunoprecipitation followed by qRT-PCR with gene-specific primers. *mec-7* and *mec-12* encode touch neuron-specific β- and α-tubulins, respectively (Tang and Jin, 2018). Loss of *mbl-1* function in the PLM and ALM mechanosensory neurons results in a truncated axon phenotype, which is recapitulated in the *mec-7* and *mec-12* single mutants but not enhanced in the *mbl-1; mec-7* and *mbl-1; mec-12* double mutants. Likewise, overexpression of *mec-7* or *mec-12* in the PLM neuron in an *mbl-1* null background rescues the axon truncation phenotype. This suggests that MBL-1 mediates PLM and ALM axon outgrowth by interacting with the *mec-7* and *mec-12* transcripts. However, *mec-7* and *mec-12* encode only one isoform; therefore, MBL-1 does not regulate these mRNA through its canonical function as a splicing factor. Rather, Puri *et al.* (2023) show that MBL-1 regulates the stability of *mec-7* and *mec-12* mRNAs by monitoring their rate of degradation in wild-type and mutant worms, suggesting that the axon truncation phenotype is a product of reduced MEC-7 and MEC-12 expression in *mbl-1* animals. Importantly, MEC-7 and MEC-12 protein levels were evaluated using a translational reporter construct, which showed significant depletion of both protein products in the *mbl-1* mutant. *mbl-1* regulates microtubule polarity and dynamics in the PLM axonal process. In wild-type animals, the axon of the PLM neuron displays majority plus-end-out oriented microtubules while the dendrite of the PLM neuron displays a random assortment of plus- and minus-end-out oriented microtubules. Loss of *mbl-1* function does not affect microtubule polarity in the dendrite; however, the axon becomes more dendrite-like with

a greater percentage of minus-end-out oriented microtubules. Furthermore, the number of growing microtubules, labeled using an EBP-2::GFP reporter, is significantly increased in the axon of the *mbl-1* mutant, signifying decreased microtubule stability and increased dynamics. It is unclear whether decreased *mec-7* and *mec-12* transcript levels mediate these effects on the microtubule cytoskeleton. Reduced availability of MEC-7 and MEC-12 building blocks may cause axonal truncation directly or indirectly by disrupting microtubule polarity and stability. Overall, these findings indicate a novel role for *mbl-1* in regulating the microtubule cytoskeleton (Puri et al., 2023).

RNAi-mediated knockdown of *muscleblind* (*mbl*) results in dendrite patterning defects in the *D. melanogaster* larval class IV da sensory neurons. These defects are characterized by an increase in terminal branching, a reduction in total dendrite length, and incomplete coverage of the sensory field (Olesnicky et al., 2014). Loss of *C. elegans mbl-1* activity causes PVD sensory neuron dendrite patterning defects characterized by fewer dendritic branches at all orders (Antonacci et al., 2015). Using a $P_{mbl\text{-}1}$::*mbl-1::*GFP (cDNA) transgene, Antonacci *et al.* (2015) revealed endogenous *mbl-1* expression within the PVD neuron and tight nuclear localization of MBL-1 protein, in agreement with the predicted function of *mbl-1* as a regulator of alternative splicing. It is unknown whether MBL-1 exhibits cytoplasmic localization in the P/ALM mechanosensory neurons where it is purported to increase the stability of *mec-7* and *mec-12* mRNA (Puri et al., 2023). Driving expression of *mbl-1* cDNA in an *mbl-1* mutant background with a pan-neuronal promoter ($P_{rab\text{-}3}$) rescues the PVD mutant phenotype while expressing *mbl-1* cDNA under the control of a muscle-specific promoter had no effect (unpublished data). These results demonstrate a cell-autonomous function for *mbl-1* within the PVD neuron.

In the current study, we extend on previous results by showing that loss of *mbl-1* function in the PVD neuron causes a reduction in terminal branching that becomes more severe with increasing distance from the neuronal cell body. We show that *mbl-1* function is not required for the stereotyped patterning of PVD muscle-skin interface innervation or the development of body wall muscle macrostructure, and that *mbl-1* does not regulate 3° branch coverage of the anterior PVD sensory field. Interestingly, we tested *mec-8* and *msi-1* loss-of-function mutants for PVD dendrite defects and found the activity of these RBPs to be dispensable during dendrite pattern formation. This suggests that, in contrast to the ALM touch neurons and the GABAergic motor neurons, either alternative splicing of *sad-1* is not required in the PVD neuron for dendrite patterning or *sad-1* alternative splicing in the PVD neuron is not regulated by *mec-8* or *msi-1*. Further, we confirm the previous finding that the P/ALM and P/AVM touch receptor neurons have truncated axons in the mutant worm and that the PLM neuron displays a defect in synapse positioning (Puri et al., 2023). We extend these results on the touch receptor neurons by showing that the PLM neuron displays an elongated dendritic process in the *mbl-1* mutant. We have generated a RAB-3::mCherry transgene that will allow us to visualize synaptic vesicles in PVD neurons to investigate whether defects in pre-synaptic component localization observed in the DA9 motor neurons extend to the PVDs. We have also generated a MEC-7::mCherry transgene to test whether overexpression of the touch neuron-specific β-tubulin MEC-7 in the PVD neurons can rescue PVD defects associated with loss of *mbl-1* function. We are in the

process of examining strains expressing these transgenes and have images showing RAB-3::mCherry puncta in the PVD axons of control worms. *mbl-1* encodes an RNA-binding protein that is predicted to regulate alternative splicing; to learn more about the molecular function of MBL-1 protein, we are biochemically isolating direct RNA targets of MBL-1 using an RNP immunoprecipitation sequencing (RIP-seq) approach.

RESULTS AND DISCUSSION

mbl-1 regulates distal terminal dendritic branch formation in PVD sensory neurons

To study dendrite patterning in the multidendritic PVD sensory neuron, we expressed GFP under the control of a PVD-specific promoter *($P_{F49H12.4}$::GFP)* and imaged immobilized young adult worms using an epifluorescence compound microscope. Previously, Antonacci *et al.* (2015) reported a PVD dendrite patterning defect associated with the *mbl-1(tm1563)* genetic mutant, quantitatively describing a reduction in 2°, 3°, and terminal PVD dendrite branching in the mutant worm (the *tm1563* null allele was used for all experiments reported in this section - future reference to the *mbl-1* mutant denotes strains containing this allele; Figure 4B). Antonacci *et al.* (2015) also noted that terminal branch loss in the *mbl-1* mutant exhibits a nuclear-distance dependency: terminal PVD branching appears grossly
normal near the neuronal cell body, while distal regions of the dendritic tree exhibit severely reduced branching.

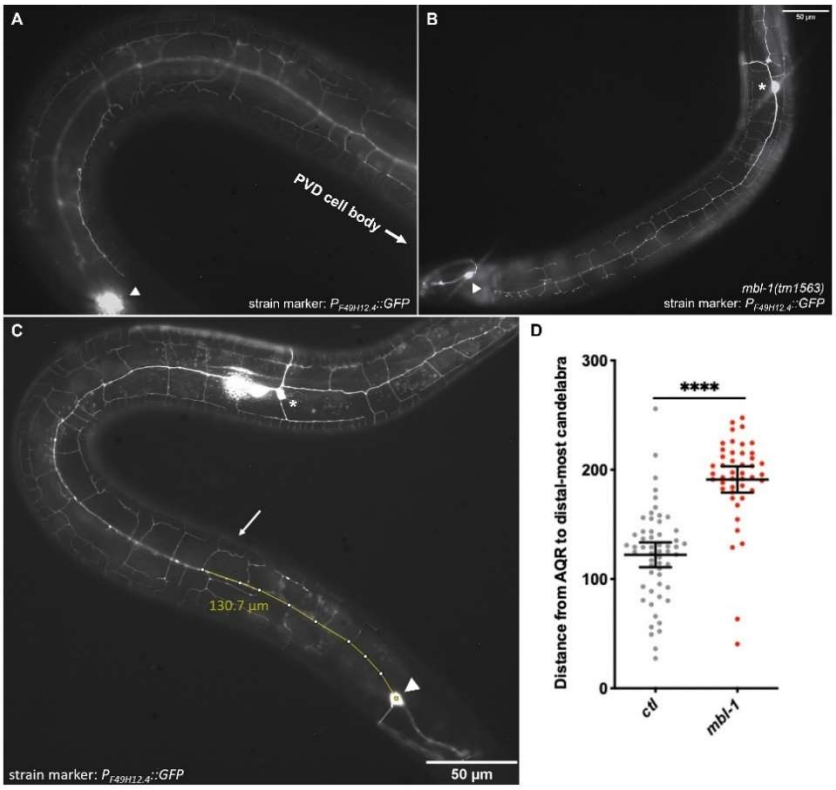

Fig 4. Distal PVD terminal branching is disrupted in the *mbl-1(tm1563)* null mutant. (A, B) Lateral view of wild-type (A) and mutant (B) animals showing the anterior dendritic arbor of the PVD neuron (arrowhead denotes the AQR soma in the head; asterisk denotes the PVD cell body). Distal-anterior terminal branching is reduced in the *mbl-1* mutant. (C) Schematic showing the method used to quantify the nuclear-distance dependency of terminal dendritic branch loss in the *mbl-1* mutant. ImageJ was used to measure the average distance between the distal-most 'true' candelabra (defined by the presence of at least two terminal branches ≥ 3µm in length; arrow) and the anterior terminus of the PVD dendritic arbor (approximated to co-localize with the cell body of the AQR neuron; arrowhead). (D) Quantification of distal terminal branch loss for wild-type (*ctl*) and mutant (*mbl-1*) animals. PVD neuron morphology was visualized in the *wdIs52* transgenic strain by epifluorescence microscopy. Points within each scatter column represent measurements taken from each side of an individual neuron or from independent animals. n (wild-type/mutant) = 56/44. Error bars represent 95% confidence interval. ****$P < 0.0001$, unpaired *t*-test.

Here, we report a quantitative assessment of PVD terminal branch loss in the *mbl-1* mutant, showing that dendritic terminal branching in the region of the PVD neuron

anterior to the cell body tapers off with increasing distance from the cell body (Figure 4). Specifically, the average distance between the distal-most 'true' candelabra (defined by the presence of at least two terminal branches ≥ 3μm in length) and the anterior terminus of the PVD dendritic arbor (approximated to co-localize with the cell body of the AQR neuron) increased by approximately 59% from 122.2 ± 11.0 μm in wild-type animals to 194.5 ± 9.7 μm in *mbl-1* mutants (95% confidence interval, $P < 0.0001$, unpaired *t*-test; Figure 4D). The fact that the degree of terminal branch loss is dependent on distance from the PVD cell body, the site of transcription, is consistent with a post-transcriptional role for MBL-1 in the regulation of mRNA transport, localization, or local translation. However, *mbl-1* encodes a tandem CCCH zinc finger domain RNA-binding protein predicted to function as a regulator of alternative splicing and, using a translational reporter for the predominant MBL-1 spliceform, Antonacci *et al.* (2015) reveal tight nuclear localization of MBL-1 protein within the PVD nucleus. Therefore, it is unlikely that MBL-1 is directly involved in mRNA processing within the dendritic tree; rather, *mbl-1* might function upstream in the regulation of these events.

mbl-1 regulates 3° dendritic branch length and number; however, loss of *mbl-1* function does not impact 3° branch coverage of the PVD sensory field

Previously, Antonacci *et al.* (2015) reported a statistically significant reduction in 2°, 3°, and terminal branching of the PVD dendritic arbor upon loss of *mbl-1* function. The observed loss of terminal branching has obvious implications for the mechanosensory and proprioceptive functions of the PVD neuron and it might also be expected that the concurrent reduction in lower-order branch number exacerbates these functional defects by producing additional gaps in PVD receptive field coverage. However, the fact that 3° branch length in wild-type PVD neurons is regulated by contact-dependent sister dendrite self-avoidance, where 3° branches extend outwards until they contact a neighboring branch which triggers them to withdraw marginally and stabilize, prompted us to ask whether the reduction in 3° branch number associated with loss of *mbl-1* function might drive compensatory 3° branch elongation (Smith et al., 2010; Figure 5).

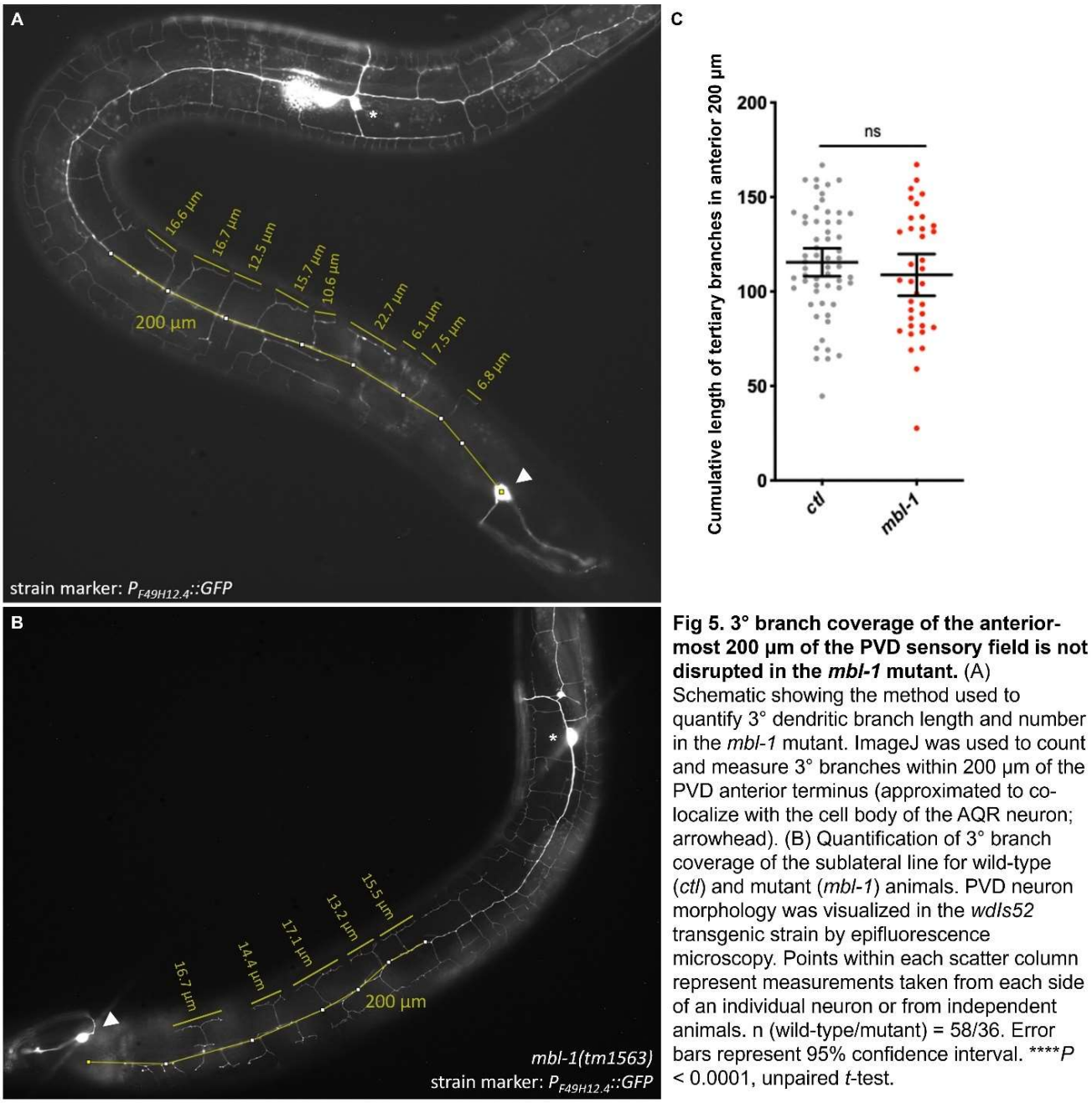

Fig 5. 3° branch coverage of the anterior-most 200 µm of the PVD sensory field is not disrupted in the *mbl-1* mutant. (A) Schematic showing the method used to quantify 3° dendritic branch length and number in the *mbl-1* mutant. ImageJ was used to count and measure 3° branches within 200 µm of the PVD anterior terminus (approximated to co-localize with the cell body of the AQR neuron; arrowhead). (B) Quantification of 3° branch coverage of the sublateral line for wild-type (*ctl*) and mutant (*mbl-1*) animals. PVD neuron morphology was visualized in the *wdIs52* transgenic strain by epifluorescence microscopy. Points within each scatter column represent measurements taken from each side of an individual neuron or from independent animals. n (wild-type/mutant) = 58/36. Error bars represent 95% confidence interval. ****$P < 0.0001$, unpaired *t*-test.

Unexpectedly, we find that within 200 µm of the PVD anterior terminus (approximated to co-localize with the cell body of the AQR neuron), average 3° branch length is decreased by approximately 29% from 21.15 ± 1.7 µm (n=317) in wild-type animals to 15.02 ± 0.8 µm (n=446) in *mbl-1* mutants (95% confidence interval, $P < 0.0001$, unpaired *t*-test). Conversely, the average number of 3° PVD branches within 200 µm of the PVD anterior terminus increased by approximately 29% from 11.0 ± 1.0 µm (n=29) in wild-type animals to 14.2 ± 1.0 µm (n=32) in *mbl-1* mutants (95% confidence interval, $P < 0.0001$, unpaired *t*-test). To determine whether these differences in 3° branch length and number impact coverage of the PVD sensory field, we calculated the cumulative

length of all 3° branches within the anterior-most 200 µm of the PVD dendritic arbor. We found that 3° branch coverage is not significantly different between wild-type and *mbl-1* animals (Figure 5B). Overall, our results support a model where contact-dependent self-avoidance dictates the length of 3° dendritic branches in the PVD neuron, ensuring complete coverage of the sublateral line. However, our findings seem to contradict the previous data showing that *mbl-1* animals exhibit reduced dendritic branching at all orders (Antonacci et al., 2015). Here, we quantified branching defects for the distal-anterior region of the mutant PVD dendritic arbor, whereas the Antonacci *et al.* (2015) study quantified dendrite patterning within the region of the PVD neuron posterior to the cell body. Taken together, these seemingly contradictory findings may suggest a model where proximity to the PVD cell body impacts the effect of *mbl-1* knockout on 2° and 3° dendritic branching, with a positive correlation between lower-order branch number and distance from the neuronal cell body. However, any conclusions drawn at this point are merely speculative due to the small sample sizes employed in our study.

Loss of *mbl-1* function does not affect the macrostructure of body wall muscle or the stereotyped patterning of PVD muscle-skin interface innervation

Previous reports have identified muscle defects in *D. melanogaster* and humans associated with the loss of MBNL family homologs (Artero et al., 1998). In fact, *muscleblind* (*mbl*) was first characterized in flies for its role in terminal photoreceptor and muscle differentiation (Artero et al., 1998; Begemann et al., 1997). Since PVD dendritic termini overlay the *C. elegans* body wall musculature and mediate the proprioceptive function of the PVD neuron by sensing muscle tension, we asked whether defects in PVD dendritic patterning might be produced cell non-autonomously in *mbl-1* mutants through effects on muscle morphogenesis. We examined muscle morphology and muscle-PVD interface organization by co-expressing cytoplasmic mCherry within the body wall muscle *(P_{myo-3}::mCherry)* and cytoplasmic GFP within the PVD neurons *($P_{F49H12.4}$::GFP)*. We could not identify any macrostructural differences between mutant and wild-type body wall muscle, although our analysis was limited to a qualitative assessment of muscle size and shape (Figure 6). In addition, besides the observed reduction in terminal branch number, innervation of the muscle-skin interface by the PVD dendritic arbor occurred normally in the *mbl-1* mutant, with 3° branches running along the lateral edges of the body wall muscle and 4° branches traversing the muscle-skin interface perpendicular to the A/P axis. Previous work by Spilker *et al.* (2012) using confocal microscopy to observe body wall muscle morphology also supports the hypothesis that *mbl-1* does not regulate muscle development in *C. elegans*, contrary to the finding that *mbl-1* is important for muscle differentiation in other organisms. To confirm that *mbl-1* functions cell autonomously in the PVD neuron, we expressed *mbl-1* cDNA in the *mbl-1* mutant under the control of pan-neuronal (P_{rab-3}) and skeletal muscle (P_{myo-3}) promoters. We witnessed significant rescue of the PVD dendritic phenotype when *mbl-1* cDNA was expressed in neurons, but not when *mbl-1* cDNA was expressed in the body wall muscle (data not shown).

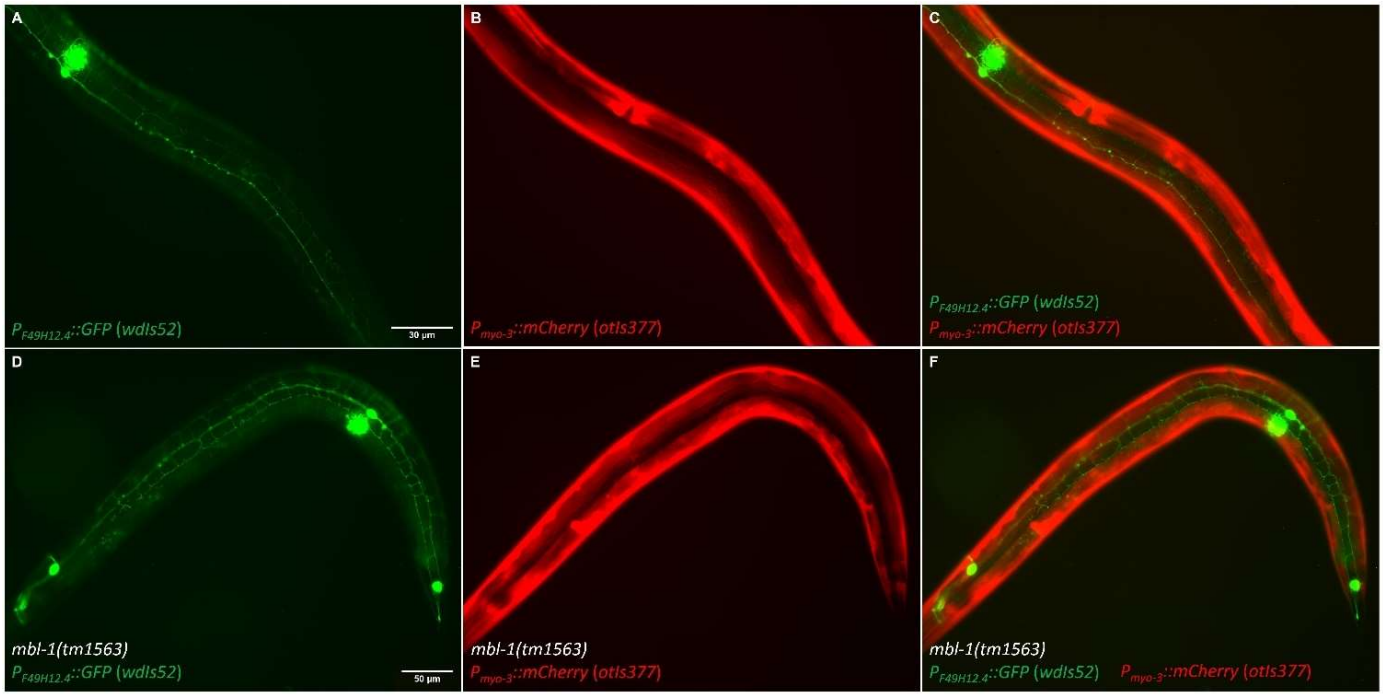

Fig 6. *mbl-1* does not regulate body wall muscle morphology in *C. elegans* nor does loss of *mbl-1* function impact the patterning of the PVD-muscle interface. (A-F) Co-expression of the $P_{F49H12.4}$::*GFP* (*wdIs52*) and P_{myo-3}::*mCherry* (*otIs377*) transgenes labels PVD neurons (green) (A,D) and body wall muscle (red) (B,E), allowing visualization of muscle morphology and the PVD-muscle interface. (C) Merged image of (A) and (B). (F) Merged image of (D) and (E). In the *mbl-1* mutant (D-F), 3° branches are observed running parallel to the body axis along the lateral edge of the body wall muscle and terminal branches are observed traversing the body wall muscle towards the dorsal nerve cord.

Loss of *mbl-1* function impacts the morphology of other mechanosensory neuron types, revealing a role for *mbl-1* in axonogenesis and synaptogenesis

Building on previous research, this study demonstrates a clear role for *mbl-1* in the establishment of the complex and stereotyped branching pattern of the PVD dendritic arbor. However, the observation that *mbl-1* is expressed broadly throughout the *C. elegans* nervous system (Antonacci et al., 2015) suggests that it may also regulate developmental processes in other *C. elegans* neurons. This notion is supported by the previous findings that *mbl-1* functions within the DA9 motor neuron as a regulator of neuromuscular junction (NMJ) synapse formation (Spilker et al., 2012) and within the ALM mechanosensory neurons as a regulator of developmentally active *sad-1* alternative splicing (Thompson et al., 2019). Since the highly branched PVD neurons are somewhat of an anomaly within the otherwise simple *C. elegans* nervous system, characterized by its plethora of unbranched neuronal processes, we asked whether *mbl-1* might possess a canonical function relevant to the development of unbranched neurites that is recapitulated within the PVD neuron to meet the increased regulatory needs of an expanded arbor.

To identify this potential canonical function of *mbl-1*, we looked for morphological defects in the six touch receptor neurons (TRNs), sensors for low-threshold mechanical stimuli, associated with loss of *mbl-1* function. The six TRNs were visualized using the MEC-4::GFP transgene, and their unbranched processes were measured. For the PLM, ALM, and AVM mechanosensory neurons, we quantified an axonal truncation phenotype associated with loss of *mbl-1* function. Specifically, we identified a 33% reduction in axonal length for the PLM neurons from 309.8 ± 46.6 µm (n=24) in wild-

type animals to 207.4 ± 27.6 μm (n=28) in *mbl-1* mutants (95% confidence interval, $P < 0.0005$, unpaired *t*-test; Figure 7), a 29% reduction in axonal length for the ALM neurons from 296.5 ± 50.9 μm (n=24) in wild-type animals to 211.6 ± 23.4 μm (n=27) in *mbl-1* mutants (95% confidence interval, $P < 0.004$, unpaired *t*-test), and a 31% reduction in axonal length for the AVM neuron from 250.0 ± 38.7 μm (n=20) in wild-type animals to 173.2 ± 30.5 μm (n=20) in *mbl-1* mutants (95% confidence interval, $P < 0.005$, unpaired *t*-test). While the ALM and AVM neurons are unipolar, with a single anterior process functioning as their axon, the PLM mechanosensory neurons elaborate two processes, an anterior axonal process and a shorter posterior dendritic process that extends into the tip of the tail. For the PLM posterior process, we quantified a dendritic elongation phenotype associated with loss of *mbl-1* function. Specifically, we identified a 43% increase in dendritic length from 36.7 ± 7.4 μm (n=25) in wild-type animals to 64.5 ± 9.9 μm (n=33) in *mbl-1* mutants (95% confidence interval, $P < 0.0001$, unpaired *t*-test). Finally, the PLM neurons extend a single synaptic branch which innervates the VNC. In wild-type animals, this synaptic branch forms from the anterior process distal to the neuronal cell body. We noticed that, in *mbl-1* animals, the location of this synaptic branch is frequently shifted towards the cell body and, in several cases, even observed its occurrence directly adjacent to the cell body. Overall, we found that 93% (26/28) of wild-type PLM neurons form distal synaptic branches while 70% (21/30) of *mbl-1* neurons form synaptic branches proximal to the cell body.

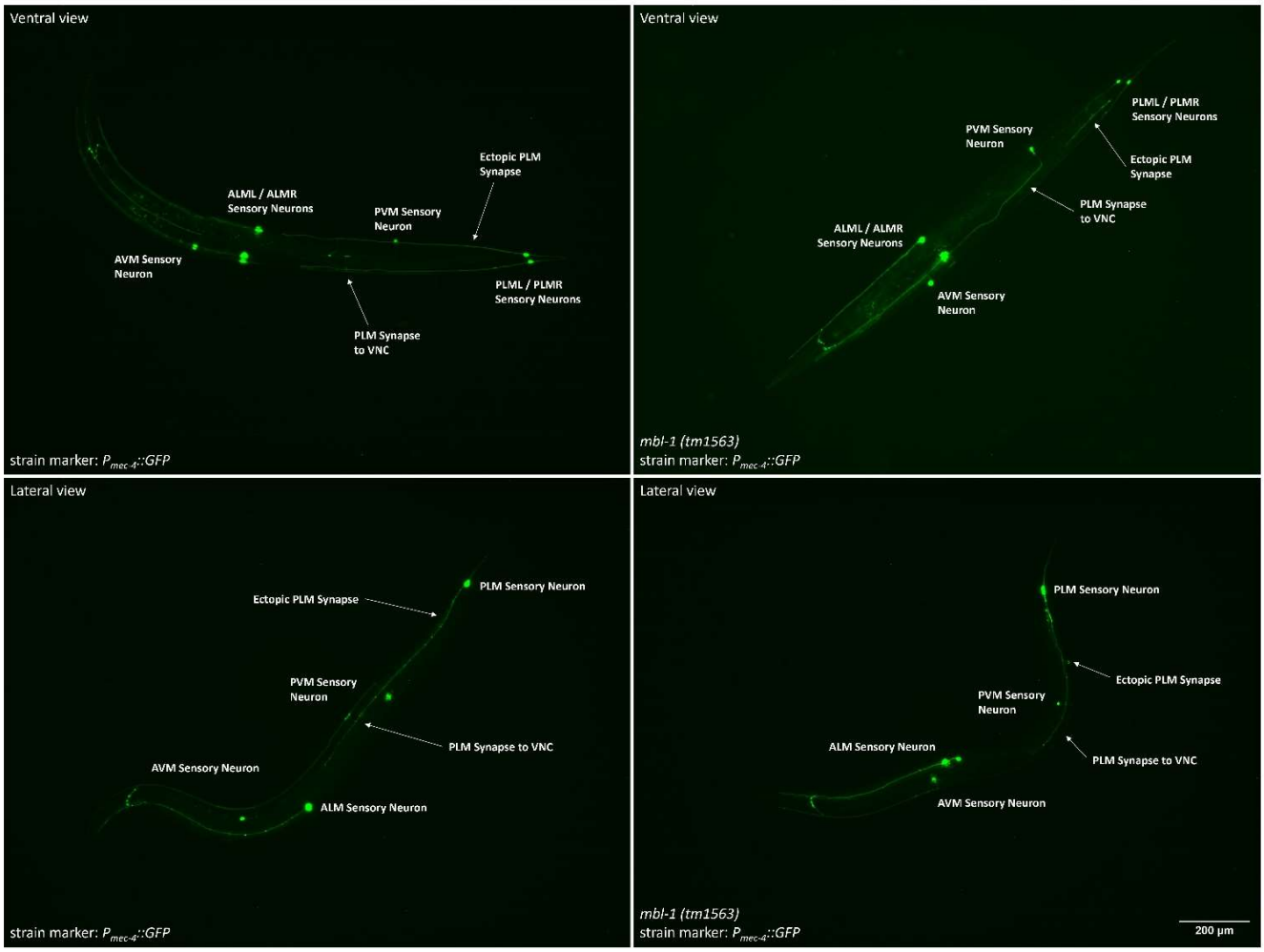

Fig 7. *mbl-1* regulates dendritogenesis, axonogenesis, and synaptogenesis within the touch receptor neurons. (A-D) The six touch receptor neurons (TRNs) were visualized in a transgenic line (*zdIs5*) that expresses cytoplasmic GFP under the control of the *mec-4* promoter. (A, B) Representative ventral views of young adult wild-type (A) and mutant (B) worms showing the general anatomy of the six touch receptor neurons. The PLM neurons form synapses onto the ventral nerve cord (VNC) which are abnormally positioned in the *mbl-1* mutant. (C, D) Representative lateral views of young adult wild-type (C) and mutant (D) worms showing morphological defects in the touch receptor neurons. Defects in neurite length are seen for the PLM, ALM, and AVM neurons. Defective synapse formation is seen for the PLM neurons.

These findings demonstrate an important role for *mbl-1* in axonogenesis and synaptogenesis, in addition to dendritogenesis. Such a broad role in neuronal morphogenesis is consistent with a model where MBL-1 regulates many developmentally relevant transcripts. The finding of dendritic elongation and axonal truncation occurring in the same neuron is counterintuitive, especially given the PVD phenotype characterized by dendritic arbor reduction, but might suggest that the *mbl-1* mutant phenotype represents a partial loss of neurite identity, with the longer PLM axonal process becoming more dendrite-like and the shorter PLM dendritic process becoming more axon-like. This model is capable of explaining the opposing phenotypes of the PLM and PVD neurons; given the relative sizes of the PVD dendrite and axon, loss of PVD dendritic identity and acquisition of axonal traits would be expected to comprise, in part, a reduction in dendritic arbor size. An interesting question to pursue next would be whether the PVD axon shows an elongated phenotype in the *mbl-1*

mutant. The PLM synapse positioning defect identified in this study is consistent with the previous finding that loss of *mbl-1* function disrupts distal NMJ synapse formation in the cholinergic DA9 motoneuron (Spilker et al., 2012). This phenotype could be explained by defects in *sad-1* alternative splicing which have been shown to occur in the PLM neurons of *mbl-1* animals and which are expected to result in synaptic organization defects given the known functions of the different *sad-1* spliceforms (Kim et al., 2010; Puri et al., 2023; Thompson et al., 2019). Broadly, this phenotype is reminiscent of a trafficking defect, a premise that is supported by the previous finding that synaptic vesicles and other pre-synaptic proteins are mislocalized within the DA9 motor neurons of *mbl-1* mutant animals (Spilker et al., 2012). To test whether a similar trafficking or transport defect is detectable within the PVD neuron, we have developed a transgene to visualize synaptic vesicle-associated RAB-3 localization within this neuron.

As a final note, previous findings on the *mbl-1* mutant phenotype in combination with our own are all explainable by the model that *mbl-1* regulates neuronal polarization and compartmentalization. RAB-3 mislocalization resulting from loss of *mbl-1* function phenotypically looks very similar to RAB-3 mislocalization in the DA9 motor neuron resulting from loss of *unc-116* function (Spilker et al., 2012; Yan et al., 2013). In addition, Yan *et al.* (2013) report dramatic elongation of the short DA9 dendritic process in the *unc-116* mutant which is highly reminiscent of the PLM neuron dendritic elongation phenotype observed in the *mbl-1* mutant. Based on this assessment, it is possible that a single direct or indirect regulatory target of MBL-1, such as a factor directly involved in the establishment of cytoskeletal polarization, could explain all of the reported phenotypic features of the *mbl-1* mutant. Fully elucidating the molecular mechanism by which *mbl-1* regulates nervous system development requires an unbiased method for studying RNA-protein interactions such as a RIP-seq, CLIP-seq, or RNA tagging-based approach.

PERSPECTIVES AND FUTURE DIRECTIONS

Our first attempt at using the RIP-seq approach to learn more about the molecular function of MBL-1 was unsuccessful – producing data that was unconducive to the extraction of meaningful insight. Specifically, high levels of non-specific RNA binding to our precipitant (i.e., high noise) coupled with very low levels of specific RNA binding to MBL-1 (i.e., low signal) precluded our ability to detect native MBL-1:RNA interactions within our sample. In cases where there was a statistically significant difference between the mock RIP group (control) and the RIP group (experimental) for a particular transcript, the prevalence of non-specific binding in the mock RIP sample, coupled with minimal amounts of specific binding in the RIP sample, precluded our ability to differentiate between specific MBL-1:RNA binding interactions and transcriptional differences produced as a result of the overexpression of *mbl-1* and *unc-76* (co-injection marker) exclusively in RIP animals. For example, we saw dramatically more *unc-76* transcript in the RIP sample likely due to the fact that *unc-76* was used as a co-injection marker during the construction of our experimental RIP strain but not during the construction of our control (GFP only) strain. However, we have not ruled out the possibility that MBL-1 and *unc-76* mRNAs interact within the cell. In addition, we observed enrichment of *mbl-1* transcript in the RIP sample, but it is unclear whether

MBL-1 regulates its own transcript or whether the overexpression of *mbl-1* in RIP animals is responsible for this result. While enrichment of *unc-76* and *mbl-1* transcripts within the RIP sample was highly significant, many other transcripts were enriched to a lesser extent. However, for all of these transcripts, it is unclear whether their enrichment in RIP animals is a product of an endogenous MBL-1:RNA interactions or differences in gene expression resulting from *mbl-1* and/or *unc-76* overexpression. Surprisingly, we found that several snoRNAs (e.g., F59C6.15) were very highly enriched in our RIP sample compared to our mock RIP sample. We have yet to explain this peculiar finding although we suspect that these MBL-1:snoRNAs interactions are non-native and rather represent an artifact of cell lysis. As part of our reasoning for this assertion, we have observed nucleolar exclusion of MBL-1::GFP in intact cells. This failure of our RIP-seq experiment to generate meaningful results could be suggestive of a general limitation of the RIP-seq approach. Immunoprecipitating an RNP complex while maintaining specific RBP:RNA interactions and minimizing non-specific RNA interactions could prove universally challenging. This is likely exacerbated by the 'stickiness' of RNA and the need to compromise between RNA purity and quantity.

Several ideas have been proposed so far for improving our RIP-seq design in the future. One possible improvement could involve scaling-up the number of mock RIP and RIP animals that we harvest to maximize the amount of initial RNA in our sample so that we have more leeway when it comes to achieving high RNA purity at the cost of loss of RNA quantity. A second improvement could involve testing several anti-GFP antibodies and performing an initial titration to determine the ideal concentration of antibody that will most efficiently pull down the MBL-1::GFP fusion. In addition, several next-generation methods for studying RNA-protein interactions that improve on the RIP-seq technique have been developed recently. One method termed CLIP-seq involves cross-linking intact cells using a chemical agent/UV irradiation prior to lysis followed by an aggressive high-salt-content wash. Positive ions in the high-salt-content wash should more efficiently dissociate negatively charged RNA non-specifically bound to the immunoprecipitated fusion protein. Cross-linking prior to lysing serves two purposes: (1) since RBP-RNA interactions can be transient and weak, the cross-linking stabilizes specific associations so that the wash can be more aggressive, (2) cross-linking prior to lysis could eliminate artifacts in the data associated with MBL-1 non-natively interacting with nucleolar/cytoplasmic cellular components after the cell/nucleus is lysed open. By crossing-linking MBL-1 to its targets while the cell is still intact, only biologically relevant interactions should show up in the data. In addition, it is possible to employ UV crosslinking that is specific to RNA-proteins interactions such that data analysis will not be complicated by the presence of protein-protein complexes and DNA-protein complexes. In particular, the existence of protein-protein interactions can make it difficult to determine whether an interaction between a protein of interest and a particular RNA transcript is a direct interaction or whether the observed interaction instead involves the RNA transcript associating with an RNP complex that contains multiple protein components. Another class of methods termed the RNA-tagging methods (e.g., TRIBE) involves creating a fusion protein of MBL-1 and an enzyme (e.g., ADAR, poly(U) polymerase) that can chemically modify RNA transcripts that it interacts closely with. A sequencing approach is used that only provides sequencing data for RNA molecules that have been chemically modified by the specific enzymatic tag.

An interesting future direction for study could be an analysis of the possible roles that MBL-1 might play in the *C. elegans* amphid chemosensory neurons (e.g., AWC, AFD). Some of these neurons have more elaborate dendritic morphologies and relatively fixed and short axons. Investigating the role of MBL-1 in regulating the elaboration of these dendritic structures could be interesting given our observations in the PVD and touch receptor neurons.

The complex and diverse cellular structures that populate the nervous systems of animals have fascinated scientists since the first descriptions of these structures were reported more than a century ago. Since then, it has been demonstrated that the complex cognitive processes and behaviors mediated by the nervous system are a product of these elaborate cellular morphologies (that is, the biological principle that structure determines function also applies to the nervous system) and, importantly, defects in the proper development of these neuronal forms are associated with a wide array of neurological disorders including autism, Alzheimer disease, schizophrenia, and bipolar disorders. Based on this understanding, a fundamental open question in neurobiology is how these cellular architectures are encoded in the genome and how cell biological processes actually drive the mechanical elaboration of these shapes. To better understand the logic behind the genetic networks that specify neuronal morphology, we are investigating the molecular function of an alternative mRNA splicing factor family known to regulate dendrite patterning in the somatosensory *C. elegans* PVD and *D. melanogaster* class IV dendritic arborization (da) neurons. By employing an RNA immunoprecipitation sequencing (RIP-seq) approach, we are attempting to generate a comprehensive list of all the direct mRNA targets of binding/regulation by the *C. elegans* homolog of this conserved splicing factor. This approach to identifying *in situ* RNA-protein interactions has the potential to help answer many additional questions related to the role of post-transcriptional gene regulation mediated by RNA-binding proteins in nervous system development.

Recent RBP genetic screens in *D. melanogaster* and *C. elegans* have made it clear that conserved RBPs play an important role in dendrite patterning, yet mechanistic explanations for how these proteins work in the neuron is lacking. Due to the relationship between dendrite morphogenesis defects and human neurological disorders, understanding the molecular functions of these RBPs could prove valuable. Gaining an unbiased and comprehensive understanding of the ways in which these RBPs regulate RNA metabolism requires protein-centric methods for studying RNA-protein interactions such as the RIP-seq approach. Through this work we demonstrate the use of the RIP-seq approach to study the molecular function of MBL-1 and discuss limitations associated with this approach, as well as potential improvements and related next-generation methods. Due to the fact that neuronal processes sometimes extend great distances from the site of transcription in the cell body and need to respond to environmental signals quickly during the process of morphogenesis, transcriptional control might not be enough to explain many morphogenetic events and post-transcriptional gene regulation mediated by RBPs could play a very important, but underappreciated role, in neuron development.

MATERIALS AND METHODS

C. elegans strains and genetics

Strains were derived from the Bristol strain N2, grown at 20°C, and constructed using standard procedures (Brenner, 1974). The *mbl-1(tm1563)* mutant allele used for all experiments was obtained from the Mitani Lab through the *C. elegans* National Bioresource Project of Japan. PVD dendrites were marked by *wdIs52[$P_{F49H12.4}$::GFP]* (Watson et al., 2008), the six touch receptor neurons (TRNs) were marked by *zdIs5[P_{mec-4}::GFP]* (Hao et al., 2001), and the body wall muscle was marked by *otIs377[P_{myo-3}::mCherry]* (Patel et al., 2012). Co-expression of the *otIs377[P_{myo-3}::mCherry]* and *wdIs52[$P_{F49H12.4}$::GFP]* markers allowed visualization of the muscle/PVD interface. All other transgenes generated for this study were constructed as described herein.

Imaging and quantification of developmental defects

Worms were picked at the young adult stage, mounted on slides with 2% (w/v) agarose pads, and immobilized with 0.6 smM levamisole. Phenotypic analysis was conducted using a 20x (TRNs and muscle/PVD interface) or 40x (PVD dendrites and muscle/PVD interface) objective on a Zeiss AxioScope.A1 epifluorescence microscope. The distance between the anterior terminus of the PVD dendritic arbor (approximated to co-localize with the cell body of the AQR neuron) and the distal-most 'true' candelabra (defined by the presence of at least two terminal branches ≥ 3μm in length) was measured using the Analyze/Measure tool in ImageJ software (http://rsbweb.nih.gov/ij/) separately on the dorsal side, the ventral side, or both. Tertiary dendrites within 200 μm of the PVD anterior terminus (approximated to co-localize with the cell body of the AQR neuron) on the dorsal and ventral sides were counted and measured using the Analyze/Measure tool in ImageJ software. Tertiary dendrite coverage of the sublateral line was calculated per animal as the cumulative length of all tertiary branches within 200 μm of the PVD anterior terminus. Body wall muscle macrostructure and muscle/PVD interface organization were assessed for qualitative defects by multiple researchers. For the PLM, ALM, and AVM touch receptor neurons, anterior neurites (axonal) were measured from the center of the neuronal cell body to the distal tip of the neurite using the Analyze/Measure tool in ImageJ. The PLM posterior neurites (dendritic) were also measured using identical methodologies. PLM synapse positioning was assessed by qualitatively categorizing synapses as 'normal' or 'ectopic' based on their position relative to the PLM cell body, the distal tip of the anterior PLM neurite, and the vulva. 'Normal' synapses were those that occurred in proximity to the neurite terminus and the vulva, while 'ectopic' synapses were those that occurred in proximity to the cell body.

Construction of transgenes and DNA microinjection

All primers used in the construction of transgenes described here are given in Table S1. *rab-3* cDNA was amplified from *otIs637[P_{bnc-1}::rab-3::GFP + P_{myo-2}::mCherry]*. Genomic DNA containing *mec-7* was amplified from the Bristol strain N2. *rab-3* and *mec-7* DNA was amplified with polymerase chain reaction (PCR) without stop codons and was cloned into the pDONR221 vector using Gateway BP Clonase II (Invitrogen). The *ser-2* promoter 3 fragment (Tsalik and Hobert, 2003) in pDONR P4-P1r and the mCherry

coding sequence with a *unc-54* 3' UTR in pDONR P2r-P3 were previously derived (Antonacci et al., 2015) using Gateway BP Clonase II (Invitrogen). *rab-3* and *mec-7* DNA, *ser-2* promoter 3, and mCherry were all cloned into pDEST R4-R3 using Gateway LR Clonase II Plus (Invitrogen).

DNA microinjection was performed using standard practices (Mello and Fire, 1995). For the RAB-3 localization study, *unc-76(e911); wdIs52* and *unc-76(e911); mbl-1(tm1563); wdIs52* hermaphrodites were injected with 20 ng/µL $P_{ser\text{-}2P3}$*::rab-3::mCherry* (cDNA) plasmid and 60 ng/µL *unc-76(+)* plasmid. For the MEC-7 overexpression study, *unc-76(e911); wdIs52* and *unc-76(e911); mbl-1(tm1563); wdIs52* hermaphrodites were injected with 20 ng/µL $P_{ser\text{-}2P3}$*::mec-7::mCherry* plasmid and 60 ng/µL *unc-76(+)* plasmid.

RNA immunoprecipitation (IP) and sequencing (RIP-Seq)

Worms containing either $P_{rab\text{-}3}$*::mbl-1::GFP* (strain DJK371) or $P_{rab\text{-}3}$*::GFP* (strain OH441) were grown on large Nematode Growth Medium (NGM) petri plates spread with *E. coli* OP50. Before starvation, worms were collected using M9 Buffer, pelleted, and immediately resuspended in 1x volume lysis buffer (10 mM Tris-HCL pH 7.5, 150 mM NaCl, 0.5 mM EDTA, 0.5% NP-40, plus addition of complete mini Roche protease inhibitor pills, Promega RNasin). Worms were frozen at -70C and then lysed by sonication (Diagenode Bioruptor) at 4C using 20 cycles of 30 sec ON (high power) and 30 sec OFF. IP was performed with GFP-Trap A fusion proteins coupled to magnetic agarose beads according to the manufacturer's protocol (Chromotek). Following IP, RNA from strain DJK371 (IP) or strain OH441 (CTL) was digested using Trizol (ThermoFisher) and chloroform (Sigma-Aldrich). Subsequently, isopropanol and GlycoBlue (ThermoFisher) were used to create a visible RNA pellet which was washed twice in 75% ethanol. RNA concentration and integrity was assessed on the TapeStation 4150 according to the manufacturer's instructions (Agilent). IP and CTL immunoprecipitations were performed synchronously and repeated for a total of three biological replicates. cDNA library preparation of the resulting RNA samples, sequencing by Illumina, and subsequent data analysis was performed by Novogene.

ACKNOWLEDGEMENTS

This work was supported by the CC Department of Molecular Biology, the CC Office of the Dean, and a CC Faculty-Student Collaborative Grant. Some strains were provided by the *Caenorhabditis* Genetics Center, which is funded by NIH Office of Research Infrastructure Programs (P40 Of010440). We are grateful to Carrie Moon, Janna Brown, Kelley Mathers, and Ruby Lamb for technical and administrative support.

I would like to express my sincere gratitude to Professor Darrell Killian, for his mentorship and support in the lab and throughout the drafting of this thesis, Professor Spencer Gang, for his invaluable suggestions and feedback on the material presented in this report, and Meena Kim, for her contributions to all aspects of this research including experimental design, data collection, and data analysis. This paper would not have been possible without the support and hard work of all of the people listed here.

LITERATURE CITED

Aguirre-Chen, C., Bülow, H.E., Kaprielian, Z., 2011. C. elegans bicd-1, homolog of the Drosophila dynein accessory factor Bicaudal D, regulates the branching of PVD sensory neuron dendrites. Development 138, 507–518. https://doi.org/10.1242/DEV.060939/-/DC1

Albeg, A., Smith, C.J., Chatzigeorgiou, M., Feitelson, D.G., Hall, D.H., Schafer, W.R., Miller, D.M., 2010. C. elegans multi-dendritic sensory neurons: Morphology and function. https://doi.org/10.1016/j.mcn.2010.10.001

Altun, Z.F. and Hall, D.H. 2024. Handbook of *C. elegans* Anatomy. In *WormAtlas*. http://www.wormatlas.org/hermaphrodite/hermaphroditehomepage.htm

Antonacci, S., Forand, D., Wolf, M., Tyus, C., Barney, J., Kellogg, L., Simon, M.A., Kerr, G., Wells, K.L., Younes, S., Mortimer, N.T., Olesnicky, E.C., Killian, D.J., 2015. Conserved RNA-binding proteins required for dendrite morphogenesis in Caenorhabditis elegans sensory neurons. G3 (Bethesda) 5, 639–653. https://doi.org/10.1534/G3.115.017327

Artero, R., Prokop, A., Paricio, N., Begemann, G., Pueyo, I., Mlodzik, M., Perez-Alonso, M., Baylies, M.K., 1998. The muscleblind gene participates in the organization of Z-bands and epidermal attachments of Drosophila muscles and is regulated by Dmef2. Dev Biol 195, 131–143. https://doi.org/10.1006/DBIO.1997.8833

Baralle, F.E., Giudice, J., 2017. Alternative splicing as a regulator of development and tissue identity. Nat Rev Mol Cell Biol. https://doi.org/10.1038/nrm.2017.27

Barington, M., Risom, L., Ek, J., Uldall, • Peter, Ostergaard, • Elsebet, 2018. A recurrent de novo CUX2 missense variant associated with intellectual disability, seizures, and autism spectrum disorder. European Journal of Human Genetics 26, 1388–1391. https://doi.org/10.1038/s41431-018-0184-5

Begemann, G., Paricio, N., Artero, R., Kiss, I., Pérez-Alonso, M., Mlodzik, M., 1997. muscleblind, a gene required for photoreceptor differentiation in Drosophila, encodes novel nuclear Cys3His-type zinc-finger-containing proteins. Development 124, 4321–4331. https://doi.org/10.1242/DEV.124.21.4321

Brenner, S., 1974. The Genetics of CAENORHABDITIS ELEGANS. Genetics 77, 71. https://doi.org/10.1093/GENETICS/77.1.71

Chatzigeorgiou, M., Yoo, S., Watson, J.D., Lee, W.H., Spencer, W.C., Kindt, K.S., Hwang, S.W., Miller, D.M., Treinin, M., Driscoll, M., Schafer, W.R., 2010. Specific roles for DEG/ENaC and TRP channels in touch and thermosensation in C. elegans nociceptors. Nature Neuroscience 2010 13:7 13, 861–868. https://doi.org/10.1038/nn.2581

Christensen, R., de la Torre-Ubieta, L., Bonni, A., Colón-Ramos, D.A., 2011. A conserved PTEN/FOXO pathway regulates neuronal morphology during C. elegans

development. Development 138, 5257–5267. https://doi.org/10.1242/DEV.069062/-/DC1

Cook, S.J., Jarrell, T.A., Brittin, C.A., Wang, Y., Bloniarz, A.E., Yakovlev, M.A., Nguyen, K.C.Q., Tang, L.T.H., Bayer, E.A., Duerr, J.S., Bülow, H.E., Hobert, O., Hall, D.H., Emmons, S.W., 2019. Whole-animal connectomes of both Caenorhabditis elegans sexes. Nature 2019 571:7763 571, 63–71. https://doi.org/10.1038/s41586-019-1352-7

Cubelos, B., Sebastiá N-Serrano, A., Beccari, L., Calcagnotto, M.E., Cisneros, E., Kim, S., Dopazo, A., Alvarez-Dolado, M., Redondo, J.M., Bovolenta, P., Walsh, C.A., Nieto, M., 2010. Article Cux1 and Cux2 Regulate Dendritic Branching, Spine Morphology, and Synapses of the Upper Layer Neurons of the Cortex. Neuron 66, 523–535. https://doi.org/10.1016/j.neuron.2010.04.038

De León, M.B., Cisneros Vega, B., 2008. Myotonic dystrophy 1 in the nervous system: From the clinic to molecular mechanisms. J Neurosci Res 86, 18–26. https://doi.org/10.1002/JNR.21377

Dong, X., Liu, O.W., Howell, A.S., Shen, K., 2013. An extracellular adhesion molecule complex patterns dendritic branching and morphogenesis. Cell 155, 296. https://doi.org/10.1016/J.CELL.2013.08.059

Egger, B., Leemans, R., Loop, T., Kammermeier, L., Fan, Y., Radimerski, T., Strahm, M.C., Certa, U., Reichert, H., 2002. Gliogenesis in Drosophila: genome-wide analysis of downstream genes of glial cells missing in the embryonic nervous system. Development 129, 3295–3309. https://doi.org/10.1242/DEV.129.14.3295

Grueber, W.B., Jan, L.Y., Jan, Y.N., 2002. Tiling of the Drosophila epidermis by multidendritic sensory neurons. Development 129, 2867–2878. https://doi.org/10.1242/DEV.129.12.2867

Hao, J.C., Yu, T.W., Fujisawa, K., Culotti, J.G., Gengyo-Ando, K., Mitani, S., Moulder, G., Barstead, R., Tessier-Lavigne, M., Bargmann, C.I., 2001. C. elegans slit acts in midline, dorsal-ventral, and anterior-posterior guidance via the SAX-3/Robo receptor. Neuron 32, 25–38. https://doi.org/10.1016/S0896-6273(01)00448-2

Herndon, L.A., Altun, Z.F., and Hall, D.H. Glossary of Anatomical Terms in *C. elegans* "U". 2013. In *WormAtlas*. doi:10.3908/wormatlas.6.1

Huang, M., Gu, G., Ferguson, E.L., Chalfiet, M., T Liu, C.D., Souza, D., K, C.R., J Neurosci, P.E., 1995. A stomatin-like protein necessary for mechanosensation in C. elegans. Nature 1995 378:6554 378, 292–295. https://doi.org/10.1038/378292a0

Hwang, R.Y., Zhong, L., Xu, Y., Johnson, T., Zhang, F., Deisseroth, K., Daniel Tracey, W., 2007. Nociceptive neurons protect Drosophila larvae from parasitoid wasps. Current Biology. https://doi.org/10.1016/j.cub.2007.11.029

Jan, Y.N., Jan, L.Y., 2010. Branching out: mechanisms of dendritic arborization. Nat Rev Neurosci 11, 316. https://doi.org/10.1038/NRN2836

Jumper, J., Evans, R., Pritzel, A., Green, T., Figurnov, M., Ronneberger, O., Tunyasuvunakool, K., Bates, R., Žídek, A., Potapenko, A., Bridgland, A., Meyer, C., Kohl, S.A.A., Ballard, A.J., Cowie, A., Romera-Paredes, B., Nikolov, S., Jain, R., Adler, J., Back, T., Petersen, S., Reiman, D., Clancy, E., Zielinski, M., Steinegger, M., Pacholska, M., Berghammer, T., Bodenstein, S., Silver, D., Vinyals, O., Senior, A.W., Kavukcuoglu, K., Kohli, P., Hassabis, D., 2021. Highly accurate protein structure prediction with AlphaFold. Nature 596. https://doi.org/10.1038/s41586-021-03819-2

Kapitein, L.C., Hoogenraad, C.C., 2011. Which way to go? Cytoskeletal organization and polarized transport in neurons. Mol Cell Neurosci 46, 9–20. https://doi.org/10.1016/J.MCN.2010.08.015

Kim, J.S.M., Hung, W., Zhen, M., 2010. The long and the short of SAD-1 kinase. Commun Integr Biol 3, 251. https://doi.org/10.4161/CIB.3.3.11455

Kulkarni, V.A., Firestein, B.L., 2012. The dendritic tree and brain disorders. Molecular and Cellular Neuroscience 50, 10–20. https://doi.org/10.1016/J.MCN.2012.03.005

Ledda, F., Paratcha, G., 2017. Mechanisms regulating dendritic arbor patterning. Cellular and Molecular Life Sciences 2017 74:24 74, 4511–4537. https://doi.org/10.1007/S00018-017-2588-8

Lee, J.E., Cooper, T.A., 2009. Pathogenic mechanisms of myotonic dystrophy. Biochem Soc Trans 37, 1281–1286. https://doi.org/10.1042/BST0371281

Liu, S., Schulze, E., Baumeister, R., 2012. Temperature- and Touch-Sensitive Neurons Couple CNG and TRPV Channel Activities to Control Heat Avoidance in Caenorhabditis elegans. PLoS One 7, e32360. https://doi.org/10.1371/JOURNAL.PONE.0032360

Lonsdale, J., Thomas, J., Salvatore, M., Phillips, R., Lo, E., Shad, S., Hasz, R., Walters, G., Garcia, F., Young, N., Foster, B., Moser, M., Karasik, E., Gillard, B., Ramsey, K., Sullivan, S., Bridge, J., Magazine, H., Syron, J., Fleming, J., Siminoff, L., Traino, H., Mosavel, M., Barker, L., Jewell, S., Rohrer, D., Maxim, D., Filkins, D., Harbach, P., Cortadillo, E., Berghuis, B., Turner, L., Hudson, E., Feenstra, K., Sobin, L., Robb, J., Branton, P., Korzeniewski, G., Shive, C., Tabor, D., Qi, L., Groch, K., Nampally, S., Buia, S., Zimmerman, A., Smith, A., Burges, R., Robinson, K., Valentino, K., Bradbury, D., Cosentino, M., Diaz-Mayoral, N., Kennedy, M., Engel, T., Williams, P., Erickson, K., Ardlie, K., Winckler, W., Getz, G., DeLuca, D., Daniel MacArthur, Kellis, M., Thomson, A., Young, T., Gelfand, E., Donovan, M., Meng, Y., Grant, G., Mash, D., Marcus, Y., Basile, M., Liu, J., Zhu, J., Tu, Z., Cox, N.J., Nicolae, D.L., Gamazon, E.R., Im, H.K., Konkashbaev, A., Pritchard, J., Stevens, M., Flutre, T., Wen, X., Dermitzakis, E.T., Lappalainen, T., Guigo, R., Monlong, J., Sammeth, M., Koller, D., Battle, A., Mostafavi, S., McCarthy, M., Rivas, M., Maller, J., Rusyn, I., Nobel, A., Wright, F., Shabalin, A., Feolo, M., Sharopova, N., Sturcke, A., Paschal, J., Anderson, J.M., Wilder, E.L., Derr, L.K., Green, E.D., Struewing, J.P., Temple, G., Volpi, S., Boyer, J.T., Thomson, E.J., Guyer, M.S., Ng, C., Abdallah, A., Colantuoni, D., Insel, T.R., Koester, S.E., A Roger Little, Bender, P.K., Lehner, T.,

Yao, Y., Compton, C.C., Vaught, J.B., Sawyer, S., Lockhart, N.C., Demchok, J., Moore, H.F., 2013. The Genotype-Tissue Expression (GTEx) project. Nat Genet. https://doi.org/10.1038/ng.2653

Mello, C., Fire, A., 1995. DNA Transformation.

Olesnicky, E.C., Antonacci, S., Popitsch, N., Lybecker, M.C., Titus, M.B., Valadez, R., Derkach, P.G., Marean, A., Miller, K., Mathai, S.K., Killian, D.J., 2018. Shep interacts with posttranscriptional regulators to control dendrite morphogenesis in sensory neurons. Dev Biol 444, 116–128. https://doi.org/10.1016/J.YDBIO.2018.09.022

Olesnicky, E.C., Killian, D.J., 2020. The cytoplasmic polyadenylation element binding protein (CPEB), Orb, is important for dendrite development and neuron fate specification in Drosophila melanogaster. Gene 738. https://doi.org/10.1016/J.GENE.2020.144473

Olesnicky, E.C., Killian, D.J., Garcia, E., Morton, M.C., Rathjen, A.R., Sola, I.E., Gavis, E.R., 2014. Extensive use of RNA-binding proteins in Drosophila sensory neuron dendrite morphogenesis. G3 (Bethesda) 4, 297–306. https://doi.org/10.1534/G3.113.009795

Park, S., Phukan, P.D., Zeeb, M., Martinez-Yamout, M.A., Dyson, H.J., Wright, P.E., 2017. Structural Basis for Interaction of the Tandem Zinc Finger Domains of Human Muscleblind with Cognate RNA from Human Cardiac Troponin T. Biochemistry 56. https://doi.org/10.1021/acs.biochem.7b00484

Pascual, M., Lidon, V., Artero, M.R., 2006. The Muscleblind family of proteins: an emerging class of regulators of developmentally programmed alternative splicing. Differentiation. https://doi.org/10.1111/j.1432-0436.2006.00060.x

Pascual, M., Vicente-Crespo, M., Fernandez-Costa, J.M., Garcia-Lopez, A., Monferrer, L., Eugenia Miranda, M., Zhou, L., Artero, R.D., 2008. Drosophila Muscleblind Is Involved in troponin T Alternative Splicing and Apoptosis. https://doi.org/10.1371/journal.pone.0001613

Patel, T., Tursun, B., Rahe, D.P., Hobert, O., 2012. Removal of Polycomb Repressive Complex 2 makes C. elegans germ cells susceptible to direct conversion into specific somatic cell types. Cell Rep 2, 1178. https://doi.org/10.1016/J.CELREP.2012.09.020

Pimentel, J., Boccaccio, G.L., Raab-Graham, K., Irma Perrone-Bizzozero, N., Willis, D.E., 2014. Translation and silencing in RNA granules: a tale of sand grains. https://doi.org/10.3389/fnmol.2014.00068

Puri, D., Sharma, S., Samaddar, S., Ravivarma, S., Banerjee, S., Ghosh-Roy, A., 2023. Muscleblind-1 interacts with tubulin mRNAs to regulate the microtubule cytoskeleton in C. elegans mechanosensory neurons. PLoS Genet 19. https://doi.org/10.1371/JOURNAL.PGEN.1010885

Rajyaguru, P., Parker, R., 2009. CGH-1 and the control of maternal mRNAs. Trends Cell Biol 19, 24–28. https://doi.org/10.1016/J.TCB.2008.11.001

Rolls, M.M., 2022. Principles of microtubule polarity in linear cells. https://doi.org/10.1016/j.ydbio.2022.01.004

Sasagawa, N., Ohno, E., Kino, Y., Watanabe, Y., Ishiura, S., 2009. Identification of Caenorhabditis elegans K02H8.1 (CeMBL), a functional ortholog of mammalian MBNL proteins. J Neurosci Res 87, 1090–1097. https://doi.org/10.1002/JNR.21942

Schachtner, L.T., Sola, I.E., Forand, D., Antonacci, S., Postovit, A.J., Mortimer, N.T., Killian, D.J., Olesnicky, E.C., 2015. Drosophila Shep and C. elegans SUP-26 are RNA-binding proteins that play diverse roles in nervous system development. Dev Genes Evol 225, 319–330. https://doi.org/10.1007/S00427-015-0514-3

Sharifnia, P., Jin, Y., Portman, D., Section, N., 2015. Regulatory roles of RNA binding proteins in the nervous system of C. elegans. https://doi.org/10.3389/fnmol.2014.00100

Smith, C.J., Watson, J.D., Spencer, W.C., O'brien, T., Cha, B., Albeg, A., Miller, D.M., 2010. Time-lapse imaging and cell-specific expression profiling reveal dynamic branching and molecular determinants of a multi-dendritic nociceptor in C. elegans. https://doi.org/10.1016/j.ydbio.2010.05.502

Spendier, K., Olesnicky, E.C., Forand, D., Wolf, M., Killian, D.J., 2021. CPB-3 and CGH-1 localize to motile particles within dendrites in C. elegans PVD sensory neurons. BMC Res Notes 14. https://doi.org/10.1186/S13104-021-05730-5

Spilker, K.A., Wang, G.J., Tugizova, M.S., Shen, K., 2012. Caenorhabditis elegans Muscleblind homolog mbl-1 functions in neurons to regulate synapse formation. Neural Dev 7. https://doi.org/10.1186/1749-8104-7-7

Stein, E., Tessier-Lavigne, M., 2001. Hierarchical organization of guidance receptors: Silencing of netrin attraction by slit through a Robo/DCC receptor complex. Science (1979) 291, 1928–1938. https://doi.org/10.1126/SCIENCE.1058445/SUPPL_FILE/INDEX.HTML

Su, C.W., Tharin, S., Jin, Y., Wightman, B., Spector, M., Meili, D., Tsung, N., Rhiner, C., Bourikas, D., Stoeckli, E., Garriga, G., Horvitz, H.R., Hengartner, M.O., 2006. The short coiled-coil domain-containing protein UNC-69 cooperates with UNC-76 to regulate axonal outgrowth and normal presynaptic organization in Caenorhabditis elegans. J Biol 5, 9. https://doi.org/10.1186/JBIOL39

Sure, G.R., Chatterjee, A., Mishra, N., Sabharwal, V., Devireddy, S., Awasthi, A., Mohan, S., Koushika, S.P., 2018. UNC-16/JIP3 and UNC-76/FEZ1 limit the density of mitochondria in C. elegans neurons by maintaining the balance of anterograde and retrograde mitochondrial transport. Sci Rep 8. https://doi.org/10.1038/S41598-018-27211-9

Tang, N.H., Jin, Y., 2018. Shaping neurodevelopment: Distinct contributions of cytoskeletal proteins. Curr Opin Neurobiol 51, 111. https://doi.org/10.1016/J.CONB.2018.02.022

Thompson, M., Bixby, R., Dalton, R., Vandenburg, A., Calarco, J.A., Norris, A.D., 2019. Splicing in a single neuron is coordinately controlled by RNA binding proteins and transcription factors. Elife 8. https://doi.org/10.7554/ELIFE.46726

Tsalik, E.L., Hobert, O., 2003. Functional Mapping of Neurons That Control Locomotory Behavior in Caenorhabditis elegans. J Neurobiol 56, 178–197. https://doi.org/10.1002/neu.10245

Verbeeren, J., Teixeira, J., Garcia, S.M.D.A., 2023. The Muscleblind-like protein MBL-1 regulates microRNA expression in Caenorhabditis elegans through an evolutionarily conserved autoregulatory mechanism. PLoS Genet 19, e1011109. https://doi.org/10.1371/JOURNAL.PGEN.1011109

Villalba, A., Coll, O., Tima Gebauer, F., Treisman, J., Richter, J., 2011. Cytoplasmic polyadenylation and translational control. Curr Opin Genet Dev. https://doi.org/10.1016/j.gde.2011.04.006

Watson, J.D., Wang, S., Von Stetina, S.E., Clay, W.C., Levy, S., Dexheimer, P.J., Kurn, N., Heath, J.D., Miller, D.M., 2008. Complementary RNA amplification methods enhance microarray identification of transcripts expressed in the C. elegans nervous system. BMC Genomics 9, 84. https://doi.org/10.1186/1471-2164-9-84

Welshhans, K., Bassell, G.J., 2011. Netrin-1-induced local β-actin synthesis and growth cone guidance requires zipcode binding protein 1. J Neurosci 31, 9800–9813. https://doi.org/10.1523/JNEUROSCI.0166-11.2011

White, J.G., Southgate, E., Thomson, J.N., Brenner, S., 1986. The structure of the nervous system of the nematode Caenorhabditis elegans. Philosophical Transactions of the Royal Society of London. B, Biological Sciences 314, 1–340. https://doi.org/10.1098/RSTB.1986.0056

Yan, J., Chao, D.L., Toba, S., Koyasako, K., Yasunaga, T., Hirotsune, S., Shen, K., 2013. Kinesin-1 regulates dendrite microtubule polarity in Caenorhabditis elegans. Elife 2. https://doi.org/10.7554/ELIFE.00133

Ye, B., Zhang, Y.W., Lily, Y.J., Yuh, N.J., 2006. The Secretory Pathway and Neuron Polarization. The Journal of Neuroscience 26, 10631. https://doi.org/10.1523/JNEUROSCI.3271-06.2006